Article

Human hippocampal neurogenesis in adulthood, ageing and Alzheimer's disease

https://doi.org/10.1038/s41586-026-10169-4

Received: 24 May 2024

Accepted: 22 January 2026

Published online: 25 February 2026

Open access

Check for updates

Ahmed Disouky[1], Mark A. Sanborn[2], K. R. Sabitha[1], Mostafa M. Mostafa[1], Ivan Alejandro Ayala[3], David A. Bennett[4], Yisha Lu[5,6], Yi Zhou[5,6], C. Dirk Keene[7], Sandra Weintraub[3], Tamar Gefen[3], M.-Marsel Mesulam[3], Changiz Geula[3], Mark Maienschein-Cline[8], Jalees Rehman[2]✉ & Orly Lazarov[1]✉

The existence of human hippocampal neurogenesis has long been disputed[1–12] and its relevance in cognition remains unknown. Recent studies have established the presence of proliferating progenitors and immature neurons and a reduction in the latter in Alzheimer's disease (AD)[11,13]. However, their origin and the molecular networks that regulate neurogenesis and function are poorly understood. Here we studied human post-mortem hippocampi obtained from different cohorts: young adults with intact memory, aged adults with no cognitive impairments, aged adults with extraordinary memory capacity (SuperAgers)[14,15], adults with preclinical intermediate pathology or adults with AD. Using multiomic single-cell sequencing (single-nucleus RNA sequencing and single-nuclei assay for transposase-accessible chromatin with sequencing), we analysed the profiles of 355,997 nuclei isolated from the hippocampus samples and identified neural stem cells, neuroblasts and immature granule neurons. Dysregulated neurogenesis was largely associated with changes in chromatin accessibility. Analyses of transcription factors and target gene signatures that distinguished each of the groups revealed early alterations in chromatin accessibility of neurogenic cells from individuals with preclinical AD, and such changes were even more evident in samples from individuals with AD. We identified a distinct profile of neurogenesis in SuperAgers that may reflect a 'resilience signature'. Finally, alterations in the profile of astrocytes and CA1 neurons govern cognitive function in the ageing hippocampus. Together, our study points to a multiomic molecular signature of the hippocampus that distinguishes cognitive resilience and deterioration with ageing.

In the rodent, the transcriptional and epigenetic mechanisms that underlie the generation of new neurons from neural stem cells (NSCs) in the subgranular layer of the dentate gyrus are well established[16]. Hippocampal neurogenesis has a crucial role in learning and memory in the rodent brain[17,18] through the recruitment of immature neurons into memory circuits to promote memory formation[19–22]. Neurogenesis is reduced as rodents age and is impaired in mouse models of AD, which contributes to memory deficits[21,23–26]. By contrast, little is known about the fate of neurogenesis in the human brain, let alone its regulatory mechanisms or functional roles in cognition. The existence of hippocampal neurogenesis in the adult human brain has generated controversy over the past few years[1,2,5,9,11,12], which is primarily attributable to limitations in the use of species-specific neurogenic proxies, sample processing, cell annotation and computational analyses[6,7,27]. There were also concerns about the overlapping molecular signatures of immature neurons and inhibitory neurons[12]. Single-nucleus RNA sequencing (snRNA-seq) studies have confirmed the existence of immature neurons in the adult human brain[11] and that there is a reduced number of immature neurons in AD[4,5,11]. A subset of progenitor cells in the adult human brain show signs of ongoing proliferation[13]. However, key knowledge gaps remain. First, the epigenetic underpinnings of neurogenesis are unknown. Defining them would facilitate an understanding of distinct capacities for neurogenesis. Second, the gene regulatory networks (GRNs) that govern neurogenesis in the adult human brain are unknown. Third, the link between neurogenesis and cognitive function in humans, and the possible impairment of neurogenesis in preclinical cases transitioning from healthy ageing to AD, remains unclear. Conversely, the characteristics of neurogenesis in persons with exceptional memory are unknown. To address these gaps, we performed multiomic snRNA-seq and single-nuclei assay for transposase-accessible chromatin with sequencing (snATAC–seq) analyses of nuclei isolated from human hippocampi from the following cohorts: young adults with intact cognition (YA); aged adults with normal-for-age cognition (HA);

[1]Department of Anatomy and Cell Biology, University of Illinois at Chicago, Chicago, IL, USA. [2]Department of Biochemistry and Molecular Genetics, University of Illinois at Chicago, Chicago, IL, USA. [3]Mesulam Center for Cognitive Neurology and Alzheimer's disease, Northwestern University, Feinberg School of Medicine, Chicago, IL, USA. [4]Rush Alzheimer's Disease Center, Chicago, IL, USA. [5]Institute of Neuroscience, State Key Laboratory of Neuroscience, CAS Center for Excellence in Brain Science and Intelligence Technology, Chinese Academy of Sciences, Shanghai, China. [6]University of Chinese Academy of Sciences, Shanghai, China. [7]UW Biorepository and Integrated Neuropathology (BRaIN) Lab, Department of Laboratory Medicine and Pathology, University of Washington, Seattle, WA, USA. [8]Research Informatics Core, University of Illinois Chicago, Chicago, IL, USA. ✉e-mail: jalees@uic.edu; olazarov@uic.edu

adults with preclinical intermediate pathology possibly transitioning from HA to AD (PCI); adults with AD; and adults termed SuperAgers (SA), who are individuals displaying exceptional performance on tests of episodic memory.

Regulatory networks of neurogenesis

To establish regulatory pathways of neurogenesis in the adult human brain, we first examined sequencing profiles of 85,977 nuclei from 8 cognitively intact adults aged 20–40 years (YA cohort; Supplementary Table 1). To ensure robust cell annotation, we used the machine learning label-transfer algorithm single-cell annotation using variational inference (scANVI)[28] implemented in single-cell variational inference (scVI)[29] to transfer labels from two human brain scRNA-seq datasets: a human developmental forebrain[30] and an adult human hippocampal dataset[11]. Unsupervised clustering based on snRNA-seq revealed 12 cell types in the hippocampus, including neuroblasts and immature neurons (Extended Data Fig. 1). The immature neurons appeared at the outer margins of the mature granule neuron cluster in a two-dimensional uniform manifold approximation and projection (UMAP) visualization. The neuroblast cluster partially overlapped with the mature oligodendrocyte (mOL) cluster. Differentially expressed genes (DEGs) and pathway analyses comparing these clusters revealed 4,166 DEGs and 169 pathways, all of which were upregulated in neuroblasts compared with mOLs. Of these, 80 pathways were associated with dendritic, axonal, postsynaptic density and neurotransmission pathways (Supplementary Table 2). Thus, to determine the nature of the similarity of these two clusters, we examined the expression levels of proxies observed in a single-cell transcriptomic-based human brain atlas[31]. We observed that oligodendrocyte-related proxies, such as myelin-associated glycoprotein (MAG) and myelin oligodendrocyte glycoprotein (MOG), were expressed in neuroblasts, albeit at lower levels than mOLs (Extended Data Fig. 2a). This finding may partially explain the visual proximity of clusters on the UMAP even though their gene expression profiles were clearly distinct.

To identify NSCs and their developmental trajectory, we examined the latent time of the astrocyte, neuroblast, immature and mature granule neuron clusters using RNA velocity. This method analyses the association between the level of cell differentiation and mRNA half-life on the basis of the ratio of nascent and mature mRNA[30]. Several subclusters were observed (Extended Data Fig. 1b). Immature neurons identified by machine learning had a lower latent time than mature granule neurons (Extended Data Fig. 1c). Two subclusters with latent times greater than astrocytes but lower than immature neurons were ascertained. One subcluster was validated as the above-identified neuroblast cluster (Extended Data Fig. 1b,c). Examination of the other subcluster compared with astrocytes revealed 766 DEGs (671 upregulated and 95 downregulated) compared with the rest of the astrocytes (Supplementary Table 3). Pathway analysis revealed that 25 out of the 65 pathways were related to neuronal development, including axonal development, node of Ranvier, initial segment, growth cone, axonal guidance, dendritic spine and postsynaptic density (Supplementary Table 3). This cluster was designated as NSCs (Extended Data Fig. 1a–c). Together, the RNA velocity analysis revealed directional flow from NSCs to an astrocyte subcluster, and then towards neuroblasts via immature neurons to mature granule neurons, a finding that supports the presence of a developmental trajectory in the adult human hippocampus (Extended Data Fig. 1b,c). Similar to what has been reported for the rodent[32], human NSCs expressed high levels of stemness proxies and low levels of neuronal markers compared with neuroblasts and immature neurons (Extended Data Fig. 1d,e). Notably, the snATAC–seq analysis enabled an orthogonal assessment of stemness via chromatin accessibility. We observed high chromatin accessibility of areas associated with multilineage potential in NSCs, whereas neuronal maturation proxies exhibited high levels of open chromatin in neuroblasts and immature neurons (Extended Data Fig. 1f). A comparison of our neurogenesis signature with previous studies that observed neurogenesis in the human dentate gyrus[13] revealed a high level of concordance (Extended Data Figs. 2–4 and Supplementary Table 4). We further validated our neurogenic signature by applying it to large scRNA-seq whole-brain datasets in which neurogenesis was not expected[33–36]. This analysis confirmed the high specificity level of our neurogenic signature (Extended Data Fig. 2).

The top DEGs and differentially accessible regions (DARs) in NSCs were downregulated in neuroblasts and further downregulated in immature neurons (Fig. 1a,b, Extended Data Fig. 5 and Supplementary Table 5). Conversely, the top DEGs and DARs in neuroblasts were downregulated in NSCs (Fig. 1a,b). Some of these genes were further upregulated in immature neurons, whereas others maintained their expression levels or were downregulated. The expression levels of the top DEGs identified in immature neurons were low in NSCs and moderate in neuroblasts, a result consistent with a transcriptomic profile shift during this trajectory (Fig. 1a,b). Developmental pathways, such as β-catenin and basolateral plasma membrane, were enriched in NSCs and downregulated in neuroblasts and immature neurons. Pathways enriched in immature neurons were related to synaptic function and plasticity (Fig. 1c and Supplementary Table 6). Motif enrichment statistics revealed that the top motifs in NSCs were those of the canonical signalling transducer family of STAT transcription factors (TFs; for example, STAT3, STAT4 and STAT5), PLAGL1 and NFIB. By contrast, in immature neurons, these were RFX2, FOS–JUN, NFE2, MEIS2 and PBX2 (Fig. 1d). This pattern suggests that there is an activity shift from TFs that promote stem cell maintenance and proliferation in NSCs to TFs that regulate neuronal differentiation and maturation in immature neurons, a finding that provides further support for a developmental trajectory in the hippocampus[37,38]. The availability of paired snRNA-seq and snATAC–seq data enabled us to determine the GRNs of neurogenesis by using the TF–peak–gene trio approach[39] and enhancer-driven GRNs (eRegulons using SCENIC+)[40]. A neurogenesis trajectory showed that the strongest interactions in NSCs were downregulated in neuroblasts and further downregulated in immature neurons. By contrast, interactions that do not exist in NSCs were mildly upregulated in neuroblasts and to a greater extent in immature neurons (Extended Data Fig. 3 and Supplementary Table 7). The magnitude of interactions changed across all cell types, whereas their direction of regulation remained consistent. Different eRegulon networks governed each cell type. The most prominent eRegulons in NSCs were *RORA*, *RORB*, *SMAD1*, *ZNF98*, *SOX6*, *PRRX1*, *NFIA*, *GLIS3*, *BCL6* and *ETV6*. In neuroblasts, these were *ZNF740*, *ZNF180*, *THRA*, *NFE2L1*, *NEUROD1*, *FEZF2*, *EGR1*, *EGR3*, *E2F1* and repressors of *NRF1*. In immature neurons, the main eRegulons were *ZNF589*, *ZNF519*, *TFDP1*, *ONECUT2*, *MTF2*, *MTA3*, *GLIS1* and *E2F3* and repressors of *SOX2* and *MXI1* (Fig. 1e and Supplementary Table 7). Together, these single-nucleus multiomic analyses establish a multifaceted molecular framework of neurogenesis in the adult human brain.

Alterations are driven by DARs

To examine the effect of age and cognitive diagnosis on neurogenesis, we sequenced nuclei isolated from the hippocampi of healthy agers with no cognitive impairments (HA cohort; $n = 8$, with 73,093 nuclei sequenced), with preclinical intermediate pathology possibly transitioning from HA to AD (PCI cohort; $n = 6$, with 58,281 nuclei sequenced) or with AD ($n = 10$, with 87,209 nuclei sequenced). Hippocampus samples from SuperAgers (SA cohort; $n = 6$, with 51,437 nuclei sequenced) were also analysed; these individuals were defined as persons aged 80 years or older whose performance on tests of episodic memory was equal to or better than that of persons aged 50–59 years[14,15]. All cell types observed in the YA group were detected in the other groups (Fig. 2a and Extended Data Fig. 4a). However, the number of NSCs was significantly

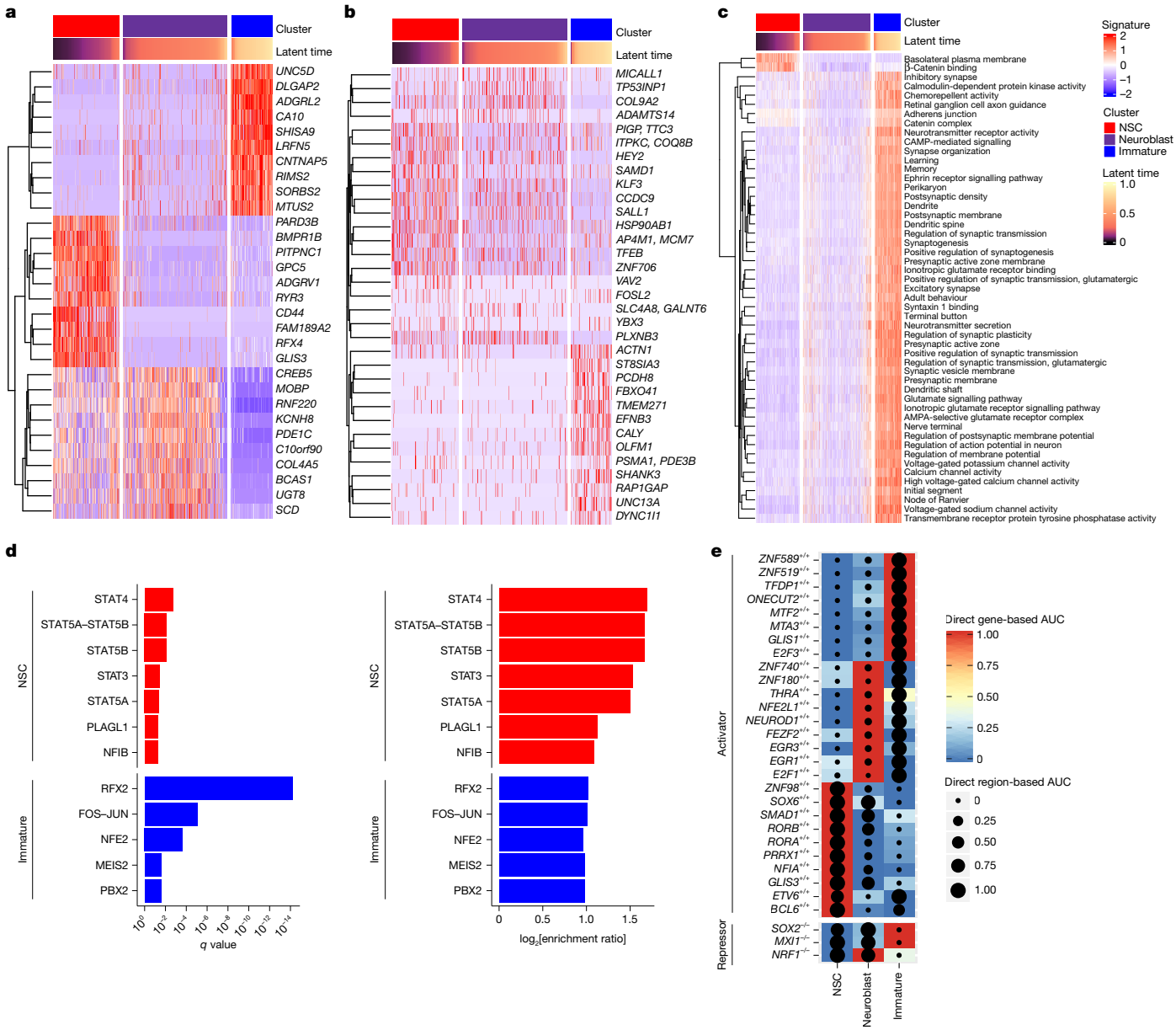

Fig. 1 | Molecular networks of neurogenesis in the adult human brain. a, The top ten DEGs for each neurogenic cell type among YA samples. **b**, The top ten DARs in gene promoters of each neurogenic cell type among YA samples. Labelled genes correspond to the overlapping promoters. Top DEGs and DARs were selected on the basis of their per cent difference in expression of all significant ($q < 0.05$) DEGs and DARs, respectively. **c**, Pathway signatures of top pathways from all neurogenesis DEGs. DEGs of the pathway analysis were based on adjusted $P < 0.01$, $\log_2$[fold change] > 1 and per cent difference > 0.3. Enriched pathways were selected on the basis of FDR < 0.05 and for nuclear gene functions for NSCs and neuroblasts. Pathways enriched in immature neurons were selected on the basis of FDR < 0.01 and $\log_2$[enrichment ratio] > 2. **d**, Motif enrichment statistics of increased open chromatin in NSCs and immature neurons. DARs were based on adjusted $P < 0.05$. Enriched motifs were selected on the basis of FDR < 0.05 and $\log_2$[enrichment ratio] > 1. **e**, Heatmap dot plot of cell-specific regulons in neurogenic cells in YA samples. The top ten most cell-specific regulons for each cell type were included if the gene-based area under the curve (AUC) change was significant (Benjamini-Hochberg (BH)-corrected, Mann–Whitney *U*-test, two-sided, FDR < 0.05).

increased in the PCI and AD groups compared with the HA cohort. Moreover, the average number of neuroblasts and immature neurons was significantly reduced in the AD group compared with the HA and YA groups. The number of immature neurons was also significantly reduced in the AD cohort compared with the PCI group (Extended Data Fig. 4b and Supplementary Table 8). The majority of age-driven and diagnosis-driven alterations in neurogenesis were observed in the number of DARs compared with DEGs, which suggests that epigenetic differences in chromatin accessibility represent a more robust molecular signature of differences in cognitive ageing than differential mRNA expression. Specifically, most DEGs were observed in NSCs, with only 172 DEGs distinguishing the AD and HA groups, 6 between AD and PCI, 154 between AD and YA and 18 between SA and the other diagnostic cohorts. The number of upregulated or downregulated DEGs and DARs in NSCs was roughly equal with age and diagnosis (Supplemental Tables 9 and 10). Examination of DEGs and DARs in all neurogenic cells combined as a function of diagnosis showed an opposite directionality of both genes and open chromatin regions in the AD group compared with the other conditions (Fig. 2b–d and Supplementary Tables 9 and 10). DAR-based motif enrichment revealed that the top motifs identified in differentially accessible chromatin regions belonged to the zinc finger TF family, whereas the most downregulated motifs belonged to the regulatory factor X (RFX) family, both of which are key drivers of development and cell growth and differentiation (Fig. 2e). Notably,

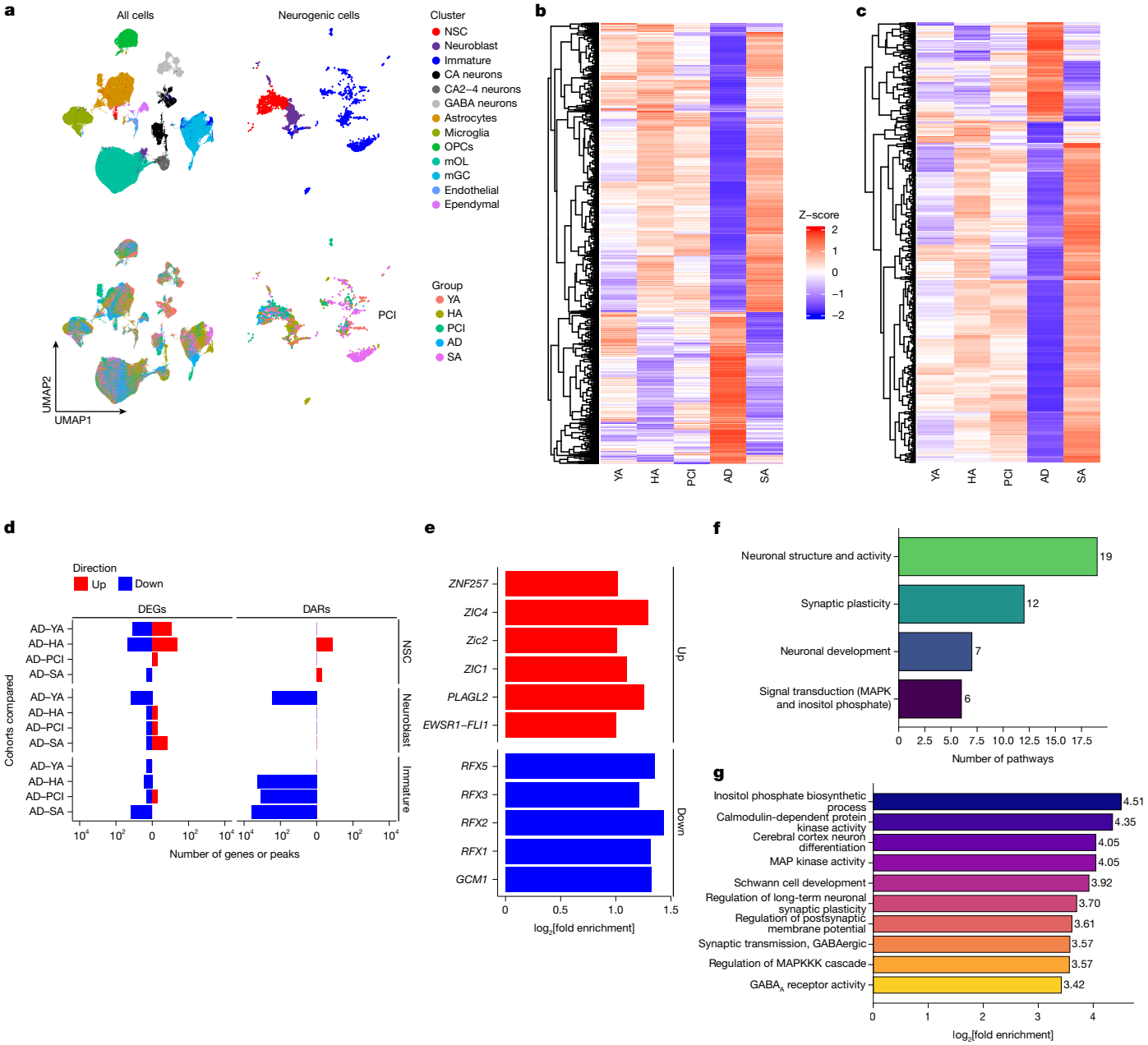

Fig. 2 | Differential expression and open chromatin with age and cognitive diagnosis. a, UMAP of all cells (left) and neurogenic cells (right), coloured by cell type (top) or diagnosis group (bottom). **b**,**c**, Heatmaps of DEGs (**b**) and DARs (**c**) in neurogenesis. **d**, The number of DEGs and DARs in neurogenesis as a function of diagnosis. **e**, Top motifs altered in neurogenesis as a function of diagnosis. **f**,**g**, Pathway enrichment analysis of inferred target genes of top DARs that were upregulated in PCI and may transition to AD through pathway abundance ($P < 0.05$; $\log_2$[fold change]) (**f**) and by $\log_2$[fold enrichment] (**g**).

we identified a set of DARs that were specifically downregulated in neuroblasts and immature neurons in the PCI cohort compared with the YA, HA and SA groups. These DARs were further downregulated in the AD group. We reasoned that such alterations in chromatin accessibility precede changes in corresponding RNA expression signatures in PCI. We integrated these peaks with the GRN analysis to identify inferred target genes, followed by pathway enrichment analysis. This process revealed that most pathways are associated with maintenance of neuronal structure and function, synaptic plasticity and neuronal development (Fig. 2f,g and Supplementary Tables 11 and 12). Together, these results suggest that downregulation of DARs induce alterations in neurogenesis as a function of cognitive deterioration and that the earliest alterations with age take place in NSCs. Moreover, most DARs and DEGs were substantially downregulated in neuroblasts and immature neurons in the AD group, and DARs associated with synaptic plasticity and neurotransmission may serve as early signatures of pathological alterations in neurogenesis.

Age and diagnosis regulatory networks

Next, we sought to determine the strongest GRNs that govern alterations in neurogenesis with ageing and disease. Using SCENIC+, which combines single-cell chromatin accessibility and gene expression data with motif discovery to infer enhancer-driven GRNs (eGRNs)[40], we determined the eRegulons of these processes. eRegulon-based UMAP visualization revealed that NSCs constituted a distinct cluster (Fig. 3a), a result that further highlights the characteristic molecular signature of NSCs at the GRN level. This finding was validated by SCENIC+ eRegulon-based diffusion[41–43], which, based on the eRegulons, revealed lineage continuity of NSCs, neuroblasts and immature neurons

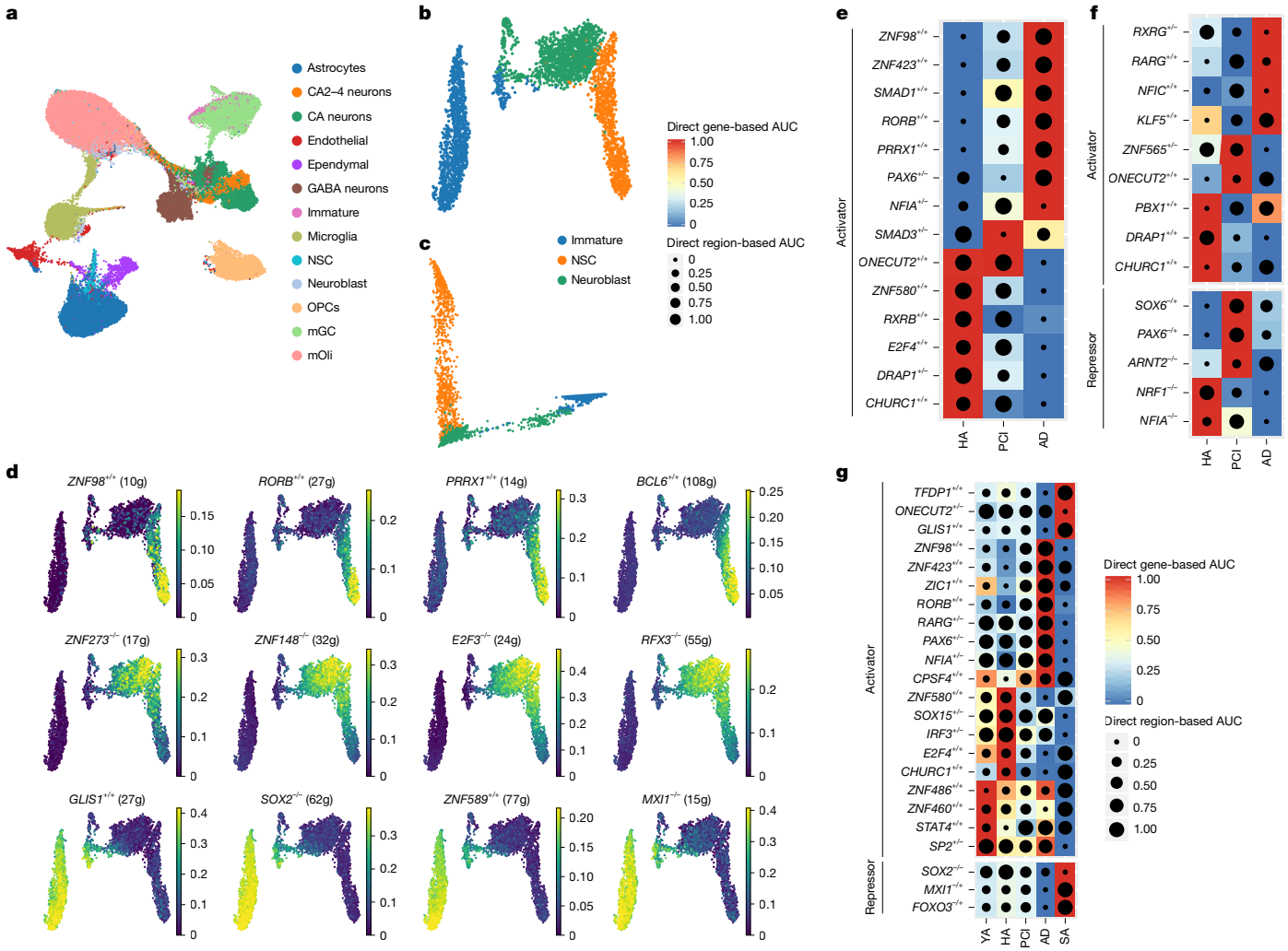

Fig. 3 | GRNs in ageing and cognitive decline. a, UMAP of all cells in every condition based on their SCENIC+ eRegulon embedding. **b**,**c**, UMAP (**b**) and diffusion map (**c**) of neurogenic cells based on their SCENIC+ eRegulon embedding. **d**, Gene-based AUC regulon activity scores projected onto the UMAP for the top four most specific regulons for each neurogenic cell type. Rows correspond to cell types as follows: top, NSCs; middle, neuroblasts; bottom, immature neurons. Colours indicate regulon activity measured as gene-based AUC scores. Only significant cell-specific eRegulons are shown (BH-corrected Mann–Whitney *U*-test, two-sided, FDR < 0.05). The number in parentheses indicates the number of target genes in each regulon (**g**). **e**, Differential regulons in all neurogenic cells for the HA, PCI and AD groups. **f**, Differential eRegulons in NSCs for the HA, PCI and AD groups. **g**, Differential eRegulons of neurogenesis in all cognitive diagnoses. For **e**–**g**, the top five regulons, based on fold change, were included for each condition if the gene-based AUC change was significant (BH-corrected, Mann–Whitney *U*-test, two-sided, FDR < 0.05).

(Fig. 3b–d and Extended Data Fig. 4c). To identify the eRegulons associated with neurogenesis in cognitive decline, we examined the top eRegulons that were altered in the PCI and AD groups compared with the HA cohort. We observed a distinct set of eRegulons that drive neurogenesis in the HA group compared with the PCI and AD conditions (Fig. 3e). Five out of the six top eRegulons that drive neurogenesis in the HA group were downregulated in the PCI and AD groups. Instead, a separate set of eRegulons was upregulated in PCI and further in AD. Notably, out of the seven upregulated eRegulons, five (*ZNF98*, *SMAD1*, *RORB*, *PRRX1* and *NFIA*) constituted the top eRegulons of NSCs in the YA cohort (Fig. 1e). This finding may partially explain the significant upregulation of NSC numbers in AD (Extended Data Fig. 4b and Supplementary Table 8). Examination of cell-type-specific eRegulons in the HA, PCI and AD groups revealed that this outcome may be due to downregulation of the *NFIA* repressor in NSCs from the PCI and AD groups compared with the HA cohort (Fig. 3f). Furthermore, distinct sets of activator and repressor eRegulons govern NSCs in these three cognitive cohorts. Specifically, *ZNF565*, *ONECUT2* activators and *SOX6*, *PAX6* and *ARNT2* repressors were upregulated in PCI. These factors were replaced by *RXRG*, *RARG*, *NFIC* and *KLF5* activators in AD (Fig. 3f). Examination of all diagnostic conditions revealed several notable findings. First, a distinct signature of SA compared with all other conditions, whereby the activators *TFDP1*, *ONECUT2* and *GLIS1* and the repressors *SOX2*, *MXI1* and *FOXO3* were upregulated. Second, a signature of activators that was uniquely upregulated in AD whereas the others were significantly downregulated, including *ZNF98*, *ZNF423*, *ZIC1*, *RORB*, *RARG*, *PAX6*, *NFIA* and *CPSF4*. Third, a signature that was driven by ageing, particularly the activators *ZNF580*, *SOX15*, *IRF3*, *E2F4* and *CHURC1* (Fig. 3g). Together, these results suggest that alterations in neurogenesis as a function of cognitive diagnosis are driven by distinct sets of combinations of GRNs that represent altered network interactions among *cis* regulatory elements, TFs and target genes.

Resilience signatures of neurogenesis

Having established that neurogenesis is altered in cognitive decline, we next sought to determine the signature of cognitive resilience, particularly in the SA cohort. Cell abundance analysis of the SA group revealed

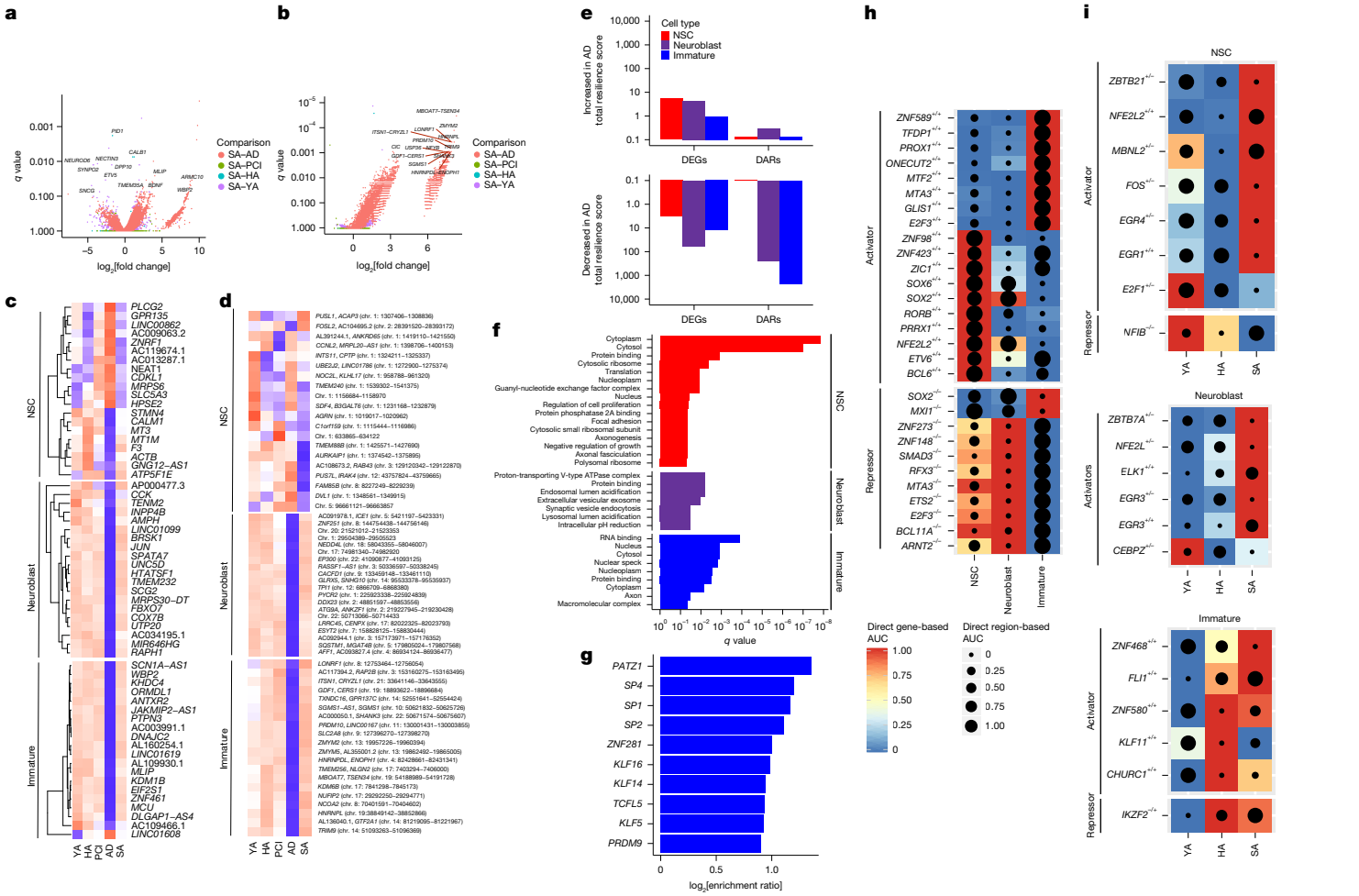

Fig. 4 | Resilience signature of neurogenesis. a,**b**, The top DEGs (**a**) and DARs (**b**) in immature neurons in SA compared with the other cognitive diagnoses. **c**,**d**, The top 20 resilience genes (**c**) and open chromatin peaks (**d**) in each cell type. **e**, Total resilience scores, summed over all genes or open chromatin peaks for each cell type, and split by the relative effect in AD: increased (top) or decreased (bottom). **f**, Pathways that are enriched in the top 500 resilience genes for each cell type (FDR < 0.05). **g**, Motifs that are enriched in the top 500 resilience open chromatin peaks for immature cells (FDR < 0.05). Note that there were no enriched motifs for NSC or neuroblast resilience peaks. **h**, Cell-specific regulons in neurogenic cells from the SA group. The top ten most cell-specific regulons for each cell type were included if the gene-based AUC change was significant (BH corrected, Mann–Whitney *U*-test, two-sided, FDR < 0.05). **i**, Differential regulons in NSCs, neuroblasts and immature neurons in the following comparisons: SA versus HA and SA versus YA. The top five regulons, based on fold change, were included for each condition if the gene-based AUC change was significant (BH corrected, Mann–Whitney *U*-test, two-sided, FDR < 0.05).

a significant increase in the number of immature neurons in the SA group compared with the other cohorts. However, we were concerned that this effect was mainly due to one outlier with a high number of immature neurons. However, even after exclusion of this sample, we observed a 2.5-fold increase in immature neurons. The abundance of immature neurons in the SA group compared with the AD cohort was significant either way. Comparisons of SA with the HA, YA and PCI cohorts showed about a twofold increase in immature neurons in the SA group, albeit this result was not significant. We further observed significantly more neuroblasts in the SA than in AD groups ($q = 0.0002$; Extended Data Fig. 4a,b and Supplementary Table 8). Examination of the neurogenesis signature in the SA group revealed that this distinct profile of immature neurons and neuroblasts can be attributed mainly to DARs. Specifically, 7,058 DARs in immature neurons and 674 in neuroblasts were upregulated in the SA cohort compared with the other groups. By contrast, few alterations were observed in NSCs (Fig. 4a,b and Supplementary Tables 9 and 10). A small number of key genes were upregulated in neuroblasts and immature neurons, such as *BDNF* (which encodes brain-derived neurotrophic factor) and *CALB1* (Fig. 4a). Downregulated genes included *NEUROD6* and *NECTIN3*, which, in association with apolipoprotein E (*APOE*), are implicated in synaptic plasticity (Fig. 4a). To confirm whether there is a resilience signature in neurogenesis, we calculated resilience scores, which were defined to identify patterns of consistent effects of DEGs and DARs in the AD group relative to the YA, HA and SA cohorts. We computed the fold change for each comparison, and the resilience score was the geometric mean of these products. A clear signature was observed in neuroblasts and immature neurons, for which most genes and peaks exhibited stable expression levels in YA, HA and SA, whereas they were substantially downregulated in AD. This pattern was particularly exaggerated in open chromatin regions (Fig. 4c–e and Supplementary Table 13). In NSCs, expression levels of some of the genes and peaks changed as a function of age or cognitive diagnosis (Fig. 4c–e). The pathways that were enriched in the top 500 resilience genes for each cell type (false discovery rate (FDR) < 0.05) in NSCs were related to cellular processes of proliferation and growth. In neuroblasts, top pathways were mitochondrial and endosomal pathway and synaptic vesicle endocytosis. In immature neurons, these were RNA binding and protein binding, cytoplasmic and axonal pathways (Fig. 4f). Motifs that were enriched in the top 500 resilience open chromatin peaks in

immature neurons included TFs of zinc finger proteins that are implicated in promoting neuronal differentiation (FDR < 0.05; Fig. 4g). To identify the strongest networks that underlie cognitive resilience, we examined the top eRegulons in the SA group. We observed a common signature of eRegulons between the YA and SA groups (Figs. 1e and 4h). Specifically, similar to the YA group, the top activators in NSCs from the SA cohort were *ZNF98*, *SOX6*, *RORB*, *PRRX1*, *ETV6* and *BCL6* and the common repressors were *SOX2* and *MXI1* (Fig. 4h). Likewise, immature neurons in the YA and SA groups shared the following common activator eRegulons: *ZNF589*, *TFDP1*, *ONECUT2*, *MTF2*, *MTA3*, *GLIS1* and *E2F3*. Common repressors were *SOX2* and *MXI1*. Samples from the SA group also exhibited unique eRegulons. Specifically, the activator eRegulon *PROX1* in immature neurons and *ZNF423*, *ZIC1*, *SOX2* and *NFE2L2* in NSCs. Moreover, NSCs from the SA group exhibited a series of repressors that are not active in the YA group. Notably, in the YA cohort, neuroblasts showed a strong differentiation-associated eRegulon signature driven by *NEUROD1*, *FEZF2*, *EGR1*, *EGR3*, *E2F1* and *THRA* (Fig. 1e). This coordinated program was entirely absent in SA, with *SOX2* and *NFE2L2* being the only activators operating in SA. Instead, neuroblasts from the SA group exhibited a series of repressors that are not active in the YA cohort. Together, this result suggests that there is a shift in the transcriptional landscape that governs neurogenesis in the YA and SA groups. (Fig. 4h). The unique eRegulon signature in the SA group was also apparent in comparison with all other diagnostic cohorts. A marked downregulation of repressors and most activators was accompanied by a strong upregulation of a specific set of eRegulons in immature neurons and neuroblasts (Extended Data Fig. 5). In neuroblasts, this included downregulation of *NEUROD1* and *NRF1* repressors concomitantly with the upregulation of *FOXO3* and *MXI1* repressors. Notably, most activators and top repressors in NSCs were downregulated, which may partially explain the scarcity of DEGs and DARs observed in NSCs from the SA group. In light of these results, we next asked whether the unique signature of SA is driven by ageing. We observed that although the profile of SA exhibited some ageing effects, most changes were independent of ageing. Specifically, in NSCs, the activator *E2F1* and the repressor *NFIB* were both downregulated in the HA and SA groups; therefore, these factors may represent ageing-induced alterations in neurogenesis. Likewise, the activator *CEBPZ*, which was dominant in the YA group, was downregulated in the HA and SA cohort. However, a unique set of eRegulons was driving NSCs and immature neurons from the SA group compared with HA, particularly upregulation of the activators *ZBTB21*, *NFE2L2*, *MBNL2*, *FOS*, *EGR4* and *EGR1* in NSCs and of *ZBTB7A*, *NFE2L1*, *ELK1* and *EGR3* in immature neurons (Fig. 4i). However, we cannot exclude the possibility that the unique eRegulons detected in samples from the SA group is the result of ageing-driven alterations. In support of this theory, the profile of neuroblasts was similar in the HA and SA groups (Fig. 4i). Together, these results highlight a specific molecular network that governs neurogenesis in SA and may contribute to cognitive superiority.

Successful or unsuccessful ageing

We next sought to determine the molecular signals that preserve hippocampal cognitive integrity (HIPPI) or that give way to pathological ageing. For this purpose, we examined signals that are differentially expressed in the SA group compared with the HA cohort and that exhibit a contrasting trend in the PCI group compared with the HA and YA groups. We observed 1,001 DEGs and 579 DARs. Most DEGs appeared in CA1 neurons, whereas most DARs appeared in astrocytes (Fig. 5a,b and Supplementary Tables 14 and 15). Significant alterations in both DEGs and DARS were also noted in oligodendrocyte progenitor cells (OPCs) and mOLs (Fig. 5a). Notably, among the most significant HIPPI in CA1 neurons were genes that have a role in neuronal function and neurotransmission (Fig. 5c); for example, *GABRB1*, *NRGN* and *KCNF*. Also notable were *APOE* in microglia, *EGR1* and *GRASP*, which link receptors, including group 1 metabotropic glutamate receptors, to neuronal proteins. The following relationships were also identified: the glutamate metabotropic receptor *GRM8* in inhibitory neurons; and *KCNE*, *GRIN2B*, *GRIA1* and *GRIK1* in mature granule cells (mGCs). Together, these results imply that the maintenance of efficient neurotransmission, synaptic plasticity and redox balance is central to the successful cognitive ageing phenotype, whereas their disruption marks the transition to PCI (Supplementary Tables 14 and 15). In addition to synapse and cellular homeostasis, pathway analysis of the HIPPI genes in CA neurons revealed cytosolic ribosome pathways, energy metabolism and mitochondrial, endosomal and lysosomal pathways (Fig. 5e). DARs in astrocytes and their motif analysis revealed numerous FOS–JUN basic leucine zipper factors (bZIP) (Fig. 5d,f). To examine the impact of the HIPPI DEGs and DARs on neurogenesis, we performed CellChat analysis among neurogenic cells, astrocytes and CA1 neuron ligand–receptor signalling. We analysed the GRN for each diagnostic group in both astrocytes and CA1 neurons and computed an 'ageing score' comparison of the same TF–peak–gene interaction strength across diagnosis groups. The most significant pathways were related to the synaptic complexes neurexin–neuroligin (NRXN1–NLGN), including the Alzheimer-related cadherin-like calsyntenin proteins (for example, NRXN1–CLSTN1 and NRXN1–CLSTN2), NCAM1, contactin (CNTN), APP–SORL1 and glutamatergic receptors (for example, Glu-SLC17, GRIAs; Glu-SLC17, GRIK2; and Glu-SLC17, GRMs) (Fig. 5g,h and Supplementary Table 16). Enhanced synaptic adhesion and glutamatergic communication in the SA and HA groups contrasted with their attenuation in the PCI and AD groups. This result suggests that preservation of excitatory synapse integrity is a hallmark of healthy cognitive ageing and a potential intervention target for the prevention of cognitive deterioration.

Discussion

Through the use of snRNA-seq and ATAC–seq of human hippocampus samples from individuals with distinct cognitive functional profiles, and integrating and analysing these data, our study provides key insights into human neurogenesis. First, we analysed the molecular network that regulates neurogenesis in the adult human hippocampus using post-mortem samples of young adults (age range of 20–40 years) with no known cognitive deficits and no dementia-related proteinopathy. We observed a neurogenic trajectory from NSCs to mature granule neurons via neuroblasts and immature neurons. The NSC cluster we identified contained several subpopulations with varying latent times, which may represent different states of NSCs and neural progenitor cells. Future analysis with greater sensitivity could facilitate an even greater resolution for the identification of NSC subpopulations. We validated the neurogenesis signature by comparing it to previous studies that observed neurogenesis in the human dentate gyrus[13] and in turn by applying it to large scRNA-seq whole-brain datasets[33–36] (Extended Data Figs. 6–8). As anticipated, the majority of brain areas in these studies showed a lack of NSCs, consistent with the notion that neurogenesis in the adult human brain is limited to areas such as the dentate gyrus of the hippocampus. Sporadic cells in other brain regions were occasionally identified as NSCs. However, given that sequenced tissue usually comes from frozen blocks that are crudely defined, we cannot exclude the possibility that these were dentate gyrus neurogenic cells that were present in brain blocks labelled as other brain regions. Our own samples were verified for the presence of the dentate gyrus in each of the frozen tissue blocks that we processed and laser-dissected for the enrichment of the dentate gyrus. Given the high variability among individuals in both studies and the different age and cognitive statuses of the participants, we conclude that our NSCs were correctly annotated.

We showed that neurogenesis is manifested by shared sets of genes, distinct signatures of chromatin accessibility and their regulatory

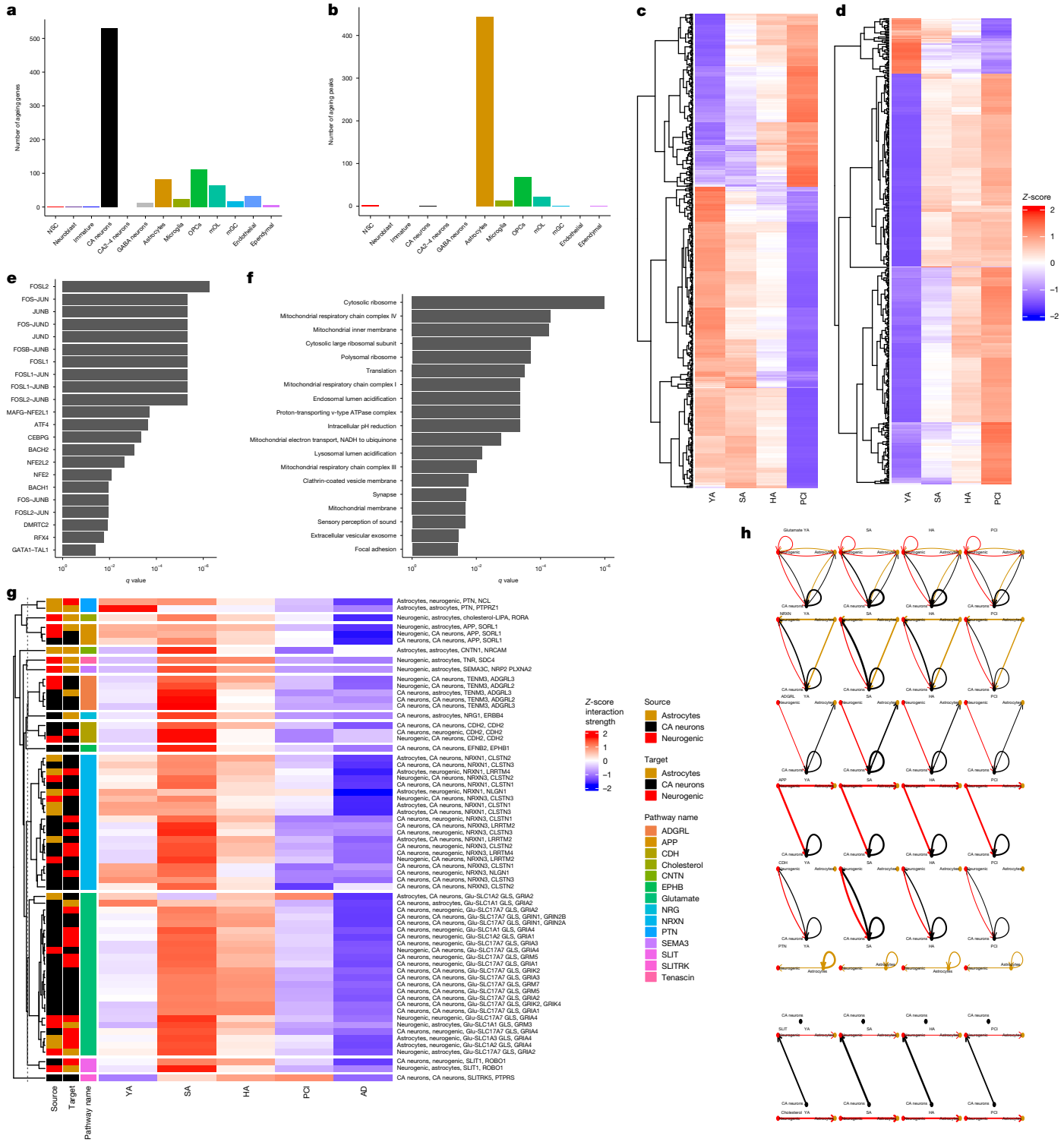

Fig. 5 | Hippocampal network in successful and unsuccessful ageing. **a**,**b**, Number of DEGs (**a**) and DARs (**b**) that show contrasting expression patterns in HA and SA compared with PCI in each cell type in the hippocampus. **c**,**d**, Heatmaps of DEGs in CA neurons (**c**) and DARs in astrocytes (**d**). **e**, Bar plot of significant pathways ($q < 0.05$) showing opposite regulation between healthy and pathological ageing (PCI) in CA neurons. **f**, Significant motifs enriched in astrocyte DARs with opposite accessibility changes between healthy and pathological ageing ($q < 0.05$ and $\log_2[\text{ratio}] > 1$). **g**,**h**, CellChat heatmap (**g**) and network plot (**h**) of the relative strength of interactions from CellChat changes from the ageing filter.

networks that clearly defined cell phenotype and maturation level. Second, we examined alterations in the regulatory networks that govern neurogenesis as a function of age and cognitive diagnosis. The earliest alterations in DEGs and DARs take place in NSCs with ageing and may give way to substantial alterations in DARs in neuroblasts and immature neurons in AD. Third, we identified DARs in PCI that may represent a molecular progression trajectory towards AD. Downregulated pathways related to these DARs were associated with synaptic plasticity and neurotransmission. Targeting them may attenuate or prevent the deterioration of neurogenesis in AD. Fourth, we identified

eRegulons associated with alterations in neurogenesis as a function of age and cognitive decline. Targeting these networks may prevent or attenuate alterations in neurogenesis, which may be manifested by the attenuation of cognitive decline. Fifth, we identified a molecular network of neurogenesis that is associated with cognitive resilience. In addition to the genes, open chromatin regions, pathways and motifs that characterized neurogenesis in SA compared with the other conditions, we examined signals in the YA and HA groups that were maintained in SA and concomitantly and significantly showed the opposite directionality in PCI and AD. This signature represents regulatory mechanisms of neurogenesis that are probably associated with the maintenance of intact cognitive function in ageing. Notably, we observed a general increase in the number of immature neurons in SA; however, inter-sample variability and low sample number compromised the power of our analysis. It should be noted that the high level of variability from sample-to-sample in cell-type abundance limited the quantitative power of our study. Future experiments with a greater number of human brain samples will be needed to study this aspect in depth. A key limitation of any multiomic analysis of human brains is the limited sample size and the large variability that is present in human brain samples. As multiomic sequencing becomes more widespread and applied to human brains with defined cognitive function, future studies will help further clarify the robustness of the differences between chromatin accessibility and mRNA expression. One explanation for the low number of DEGs versus the substantially higher number of DARs across ageing and function phenotypes could reflect the transient nature of mRNA stability depending on the differences in collection methods. By contrast, chromatin accessibility of DNA is less likely to depend on differences in collection times and procedures. Alternatively, mRNA differences could also be more indicative of acute responses of the brain to stimuli, whereas chromatin accessibility may be a more robust and consistent indicator of underlying neuronal states. Sixth, we identified that neurogenesis in SA is led by a distinct set of GRNs. Finally, we identified molecular signals in the hippocampus that promote healthy ageing with intact cognition (HIPPI) or cognitive decline. We showed that such alterations are most apparent in DEGs in CA1 neurons and DARs in astrocytes and we identified putative regulatory networks that govern these interactions. Glutamatergic pathways spearhead the interactions between CA1, astrocytes and neurogenesis and may determine the crossroad between successful and unsuccessful ageing. These alterations in the CA1 may give way to the significantly reduced number of CA1 neurons in AD. These data indicate that cell–cell interactions may have a role in memory formation and cognitive function. In summary, our study delineated the molecular signatures of hippocampal neurogenesis and their alterations as a function of age and cognitive status. The marked differences in chromatin accessibility across the neurogenic spectrum suggest that epigenetic differences represent more definitive signatures of distinct ageing-associated cognitive impairment trajectories than those observed only via gene expression analysis. This study analysed the most significant enhancer-driven GRNs by inferring the interactions between DARs and target genes and determined the molecular networks that underlie cognitive resilience. Demonstration of such epigenetic signatures associated with neurogenic cells in the human hippocampus highlights the importance of identifying the underlying molecular mechanisms for future targeted therapeutics that aim to preserve cognitive function during ageing.

Online content

Any methods, additional references, Nature Portfolio reporting summaries, source data, extended data, supplementary information, acknowledgements, peer review information; details of author contributions and competing interests; and statements of data and code availability are available at https://doi.org/10.1038/s41586-026-10169-4.

1. Sorrells, S. F. et al. Positive controls in adults and children support that very few, if any, new neurons are born in the adult human hippocampus. *J. Neurosci.* **41**, 2554–2565 (2021).
2. Sorrells, S. F. et al. Human hippocampal neurogenesis drops sharply in children to undetectable levels in adults. *Nature* **555**, 377–381 (2018).
3. Paredes, M. F. et al. Does adult neurogenesis persist in the human hippocampus? *Cell Stem Cell* **23**, 780–781 (2018).
4. Tobin, M. K. et al. Human hippocampal neurogenesis persists in aged adults and Alzheimer's disease patients. *Cell Stem Cell* **24**, 974–982 (2019).
5. Moreno-Jimenez, E. P. et al. Adult hippocampal neurogenesis is abundant in neurologically healthy subjects and drops sharply in patients with Alzheimer's disease. *Nat. Med.* **25**, 554–560 (2019).
6. Terreros-Roncal, J. et al. Methods to study adult hippocampal neurogenesis in humans and across the phylogeny. *Hippocampus* **33**, 271–306 (2023).
7. Gallardo-Caballero, M. et al. Prolonged fixation and post-mortem delay impede the study of adult neurogenesis in mice. *Commun. Biol.* **6**, 978 (2023).
8. Flor-Garcia, M. et al. Unraveling human adult hippocampal neurogenesis. *Nat. Protoc.* **15**, 668–693 (2020).
9. Boldrini, M. et al. Human hippocampal neurogenesis persists throughout aging. *Cell Stem Cell* **22**, 589–599 (2018).
10. Tartt, A. N. et al. Considerations for assessing the extent of hippocampal neurogenesis in the adult and aging human brain. *Cell Stem Cell* **23**, 782–783 (2018).
11. Zhou, Y. et al. Molecular landscapes of human hippocampal immature neurons across lifespan. *Nature* **607**, 527–533 (2022).
12. Franjic, D. et al. Transcriptomic taxonomy and neurogenic trajectories of adult human, macaque, and pig hippocampal and entorhinal cells. *Neuron* **110**, 452–469 (2022).
13. Dumitru, I. et al. Identification of proliferating neural progenitors in the adult human hippocampus. *Science* **389**, 58–63 (2025).
14. Harrison, T. M., Weintraub, S., Mesulam, M. M. & Rogalski, E. Superior memory and higher cortical volumes in unusually successful cognitive aging. *J. Int. Neuropsychol. Soc.* **18**, 1081–1085 (2012).
15. Rogalski, E. J. et al. Youthful memory capacity in old brains: anatomic and genetic clues from the Northwestern SuperAging Project. *J. Cogn. Neurosci.* **25**, 29–36 (2013).
16. Goncalves, J. T., Schafer, S. T. & Gage, F. H. Adult neurogenesis in the hippocampus: from stem cells to behavior. *Cell* **167**, 897–914 (2016).
17. Toda, T., Parylak, S. L., Linker, S. B. & Gage, F. H. The role of adult hippocampal neurogenesis in brain health and disease. *Mol. Psychiatry* **24**, 67–87 (2019).
18. Kempermann, G., Song, H. & Gage, F. H. Neurogenesis in the adult hippocampus. *Cold Spring Harb. Perspect. Biol.* **7**, a018812 (2015).
19. Marin-Burgin, A., Mongiat, L. A., Pardi, M. B. & Schinder, A. F. Unique processing during a period of high excitation/inhibition balance in adult-born neurons. *Science* **335**, 1238–1242 (2012).
20. Kee, N., Teixeira, C. M., Wang, A. H. & Frankland, P. W. Preferential incorporation of adult-generated granule cells into spatial memory networks in the dentate gyrus. *Nat. Neurosci.* **10**, 355–362 (2007).
21. Mishra, R. et al. Augmenting neurogenesis rescues memory impairments in Alzheimer's disease by restoring the memory-storing neurons. *J. Exp. Med.* **219**, e20220391 (2022).
22. Twarkowski, H., Steininger, V., Kim, M. J. & Sahay, A. A dentate gyrus–CA3 inhibitory circuit promotes evolution of hippocampal-cortical ensembles during memory consolidation. *eLife* **11**, e70586 (2022).
23. Demars, M., Hu, Y. S., Gadadhar, A. & Lazarov, O. Impaired neurogenesis is an early event in the etiology of familial Alzheimer's disease in transgenic mice. *J. Neurosci. Res.* **88**, 2103–2117 (2010).
24. Disouky, A. & Lazarov, O. Adult hippocampal neurogenesis in Alzheimer's disease. *Prog. Mol. Biol. Transl. Sci.* **177**, 137–156 (2021).
25. Hollands, C. et al. Depletion of adult neurogenesis exacerbates cognitive deficits in Alzheimer's disease by compromising hippocampal inhibition. *Mol. Neurodegener.* **12**, 64 (2017).
26. Gadadhar, A., Marr, R. A. & Lazarov, O. Presenilin-1 regulates neural progenitor cell differentiation in the adult brain. *J. Neurosci.* **31**, 2615–2623 (2011).
27. Tosoni, G. et al. Mapping human adult hippocampal neurogenesis with single-cell transcriptomics: reconciling controversy or fueling the debate? *Neuron* **111**, 1714–1731 (2023).
28. Xu, C. et al. Probabilistic harmonization and annotation of single-cell transcriptomics data with deep generative models. *Mol. Syst. Biol.* **17**, e9620 (2021).
29. Lopez, R., Regier, J., Cole, M. B., Jordan, M. I. & Yosef, N. Deep generative modeling for single-cell transcriptomics. *Nat. Methods* **15**, 1053–1058 (2018).
30. La Manno, G. et al. RNA velocity of single cells. *Nature* **560**, 494–498 (2018).
31. Chen, X. et al. A brain cell atlas integrating single-cell transcriptomes across human brain regions. *Nat. Med.* **30**, 2679–2691 (2024).
32. Habib, N. et al. Div-Seq: single-nucleus RNA-Seq reveals dynamics of rare adult newborn neurons. *Science* **353**, 925–928 (2016).
33. Siletti, K. et al. Transcriptomic diversity of cell types across the adult human brain. *Science* **382**, eadd7046 (2023).
34. Liu, Z. et al. Single-cell multiregion epigenomic rewiring in Alzheimer's disease progression and cognitive resilience. *Cell* **188**, 4980–5002 (2025).
35. Mathys, H. et al. Single-cell atlas reveals correlates of high cognitive function, dementia, and resilience to Alzheimer's disease pathology. *Cell* **186**, 4365–4385 (2023).
36. Smajic, S. et al. Single-cell sequencing of human midbrain reveals glial activation and a Parkinson-specific neuronal state. *Brain* **145**, 964–978 (2022).
37. Sugiaman-Trapman, D. et al. Characterization of the human RFX transcription factor family by regulatory and target gene analysis. *BMC Genomics* **19**, 181 (2018).
38. Schlingensiepen, K. H. et al. The role of Jun transcription factor expression and phosphorylation in neuronal differentiation, neuronal cell death, and plastic adaptations in vivo. *Cell. Mol. Neurobiol.* **14**, 487–505 (1994).

39. Anderson, A. G. et al. Single nucleus multiomics identifies ZEB1 and MAFB as candidate regulators of Alzheimer's disease-specific *cis*-regulatory elements. *Cell Genom.* **3**, 100263 (2023).
40. Bravo Gonzalez-Blas, C. et al. SCENIC+: single-cell multiomic inference of enhancers and gene regulatory networks. *Nat. Methods* **20**, 1355–1367 (2023).
41. Haghverdi, L., Buttner, M., Wolf, F. A., Buettner, F. & Theis, F. J. Diffusion pseudotime robustly reconstructs lineage branching. *Nat. Methods* **13**, 845–848 (2016).
42. Coifman, R. R. et al. Geometric diffusions as a tool for harmonic analysis and structure definition of data: diffusion maps. *Proc. Natl Acad. Sci. USA* **102**, 7426–7431 (2005).
43. Wolf, F. A., Angerer, P. & Theis, F. J. SCANPY: large-scale single-cell gene expression data analysis. *Genome Biol.* **19**, 15 (2018).

Methods

Ethics statement

The YA, HA, PCI and AD samples were obtained from the University of Washington repository bank. In 2016, the University of Washington Institutional Review Board issued an official determination that the post-mortem repository work does not meet the metric of human subject research as this study collects samples from deceased individuals. These practices are now informed by the US Revised Uniform Anatomical Gift ACT 2006 (last revised or amended in 2009) and Washington Statute Chapter 68.64 RCW. Consent forms and HIPAA compliance are regulated by the University of Washington School of Medicine Compliance Office. All materials were collected under informed consent. For the SuperAgers, written informed consent and agreement to enter the study and the brain donation programme were obtained from all participants in the study, and the study was approved by the Northwestern University Institutional Review Board and in accordance with the Helsinki Declaration.

Donor cohorts and tissues

Where applicable, all human tissue studies were approved by the institutional review boards with oversight over the specific cohort studies, and all tissue samples were obtained with informed consent. Human brain tissue samples for molecular omics and sequencing studies were provided by the University of Washington (UW) BioRepository and Integrated Neuropathology (BRaIN) laboratory, which supports a number of cohort studies that were represented in the cohort for this study, including the UW Alzheimer's Disease Research Center (ADRC) clinical core, the Kaiser Permanente Washington Health Research Institute Adult Changes in Thought (ACT) study, the Seattle Longitudinal Study (SLS) and the Pacific Northwest Brain Donor Network (PNBDN). Tissue samples were derived through a rapid tissue collection process, performed with a post-mortem interval of <12 h, and includes rapid procurement of the donor brain, coronal slicing and rapid sampling and freezing (either flash-freezing in liquid nitrogen or in supercooled dry ice and isopentane slurry), fixation of brain followed by routine sampling and diagnostic neuropathological analysis according to the National Institute on Aging and the Alzheimer's Association guidelines for the pathological assessment of AD and related dementias[44,45]. This study was designed with five groups: YA, HA, PCI, AD and SA (Supplementary Table 1).

SA cohort

All participants were required to have preserved activities of daily living and to lack clinical evidence or history of neurological or psychiatric disease. The autopsied brains of participants characterized as cognitive SuperAgers from the Northwestern SuperAging Program were obtained from the Northwestern University Alzheimer's Disease Research Center (NU-ADRC) Brain Bank. Written informed consent and agreement to enter the brain donation programme were obtained from all participants in the study, and the study was approved by the Northwestern University Institutional Review Board and in accordance with the Helsinki Declaration (https://www.wma.net/what-we-do/medical-ethics/declaration-of-helsinki/). Samples from representative brain regions of each participant were qualitatively surveyed and found to be free of significant neurodegenerative pathology other than common age-related changes. After autopsy, the right hemisphere was cut into 2–3 cm blocks and each block was flash-frozen on dry ice. Tissue at the mid-hippocampal region was collected from frozen blocks and used in this study. SA were required to be 80 years of age or older and to perform at or above average normative values for individuals in their 50s and 60s on the delayed recall of the Rey auditory verbal learning test (RAVLT)[46], and within one standard deviation of the average range for their age and education on measures of other cognitive domains according to published normative values based on age, sex and race or ethnicity[47,48].

Fresh-frozen preparation of samples and isolation of nuclei

The dentate gyrus was isolated from fresh-frozen blocks of 38 participants representing 5 diagnostic groups (YA, HA, PCI, AD and SA). Tissue was then immediately homogenized, whereby for each sample, a separate homogenizer and douncing pestles (loose and tight) were used. Each sample was homogenized in 1 ml pre-chilled lysis buffer (0.1% NP-40 alternative (or NP-40), 10 mM Tris, 146 mM NaCl, 1 mM $CaCl_2$, 21 mM $MgCl_2$ and 40 U ml^{-1} RNAse inhibitor) by mechanical douncing 20 times with the loose pestle followed by 20 times with the tight pestle to obtain a single-cell suspension. Cell suspensions were then incubated on ice for 5 min. The homogenate was then filtered through 70 µm filters (Miltenyi Biotec 130-041-407) and 40 µm filters (Miltenyi Biotec 130-041-406), moved to 1.5 ml tubes and centrifuged at 4 °C for 5 min at 500 rcf. Supernatants were removed and the nucleus pellet was washed 3 times with wash buffer (10 mM Tris, 146 mM NaCl, 1 mM $CaCl_2$, 21 mM $MgCl_2$, 0.01% BSA and 40 U ml^{-1} RNAse inhibitor). After the last wash, the supernatant was removed, and the nucleus pellet was resuspended in resuspension buffer and mixed with 900 µl Sucrose Cushion buffer. To remove additional debris, resuspended nuclei were loaded above a 3 Sucrose Cushion gradient (2.7 ml Nuclei PURE 2M Sucrose Cushion solution with 300 µl Nuclei PURE Sucrose Cushion buffer), and the sucrose gradient containing the nuclei was centrifuged at 13,000 rcf for 45 min at 4 °C. The supernatant was then carefully removed and the samples were immediately processed using the Single Cell protocol from 10x Genomics.

10x Genomics Multiome library preparation and sequencing

The 10x Genomics Multiome library preparation process and sequencing were done at Northwestern University NUseq facility core with the support of an NIH grant (1S10OD025120). The number of nuclei was analysed using Nexcelom Cellometer Auto2000 with the AOPI fluorescent staining method. The nuclei first underwent transposition with ATAC enzyme for 1 h at 37 °C. Next, 16,000 transposed nuclei were loaded into a Chromium Controller (10x Genomics, PN-120223) on a Chromium Next GEM Chip J (10x Genomics, PN-1000230), and single-cell gel beads were generated in the emulsion (GEM) according to the manufacturer's protocol. Barcoded DNA and cDNA were PCR-amplified and subjected to library construction. The snATAC–seq library was generated using a Chromium Next GEM Single Cell Multiome ATAC + Gene expression kit (10x Genomics, PN-1000281) and Single Index Kit N Set A (10x Genomics, PN-1000212) according to the manufacturer's instructions. Amplified cDNA was used for the gene expression library with a dual Index Kit TT Set A (10x Genomics, PN-1000215). Quality control for the constructed library was performed using an Agilent Bioanalyzer High Sensitivity DNA kit (Agilent Technologies, 5067-4626) and a Qubit DNA HS assay kit for qualitative and quantitative analysis, respectively. For the snATAC–seq library, the multiplexed libraries were pooled and sequenced on an Illumina Novaseq sequencer with 100 cycles kits using the following read length: 50 bp read 1 and 49 bp read 2. For the snRNA–seq library, the libraries were sequenced on an Illumina Novaseq sequencer with 100 cycles kits using the following read length: 28 bp read 1 for cell barcode and unique molecular identifiers (UMIs) and 90 bp read 2 for transcript expression. The targeted sequencing depth for snATAC–seq and snRNA-seq was 25,000 and 20,000 reads per cell, respectively.

10x single-cell multiome

Raw reads were demultiplexed and single-nucleus gene expression and peak enrichment were quantified simultaneously using CellRanger-arc count (10x Genomics). The quality of the run was assessed using the following criteria: (1) demultiplexing metrics, including the number of cells captured and the per cent of reads with valid barcodes; (2) gene expression metrics, including the per cent of mappable reads to the genome and transcriptome, and the median UMI counts and median

genes expressed per cell; and (3) open chromatin metrics, including the per cent of mappable reads to the genome, in peaks and to promoter sequences, and the median counts and total peaks observed per cell. Following the quantification and peak calling analysis for each individual sample, all captures were aggregated to obtain a unified feature set for downstream analysis using CellRanger-arc aggr (10x Genomics).

Single-cell analysis

All samples were analysed together. Single cells were filtered to ensure that data used in the downstream analysis were of high quality. Cells with >10% mitochondrial expression, indicative of dead or dying cells, cells with low numbers of genes expressed (<1,000 genes) or low total UMI RNA counts (<2,000 UMI counts) and cells with low peak numbers (<200 peaks) or total ATAC counts (<500 counts) were removed. Clustering was performed on the RNA-seq data, anticipating that gene expression would have a higher dynamic range than open chromatin, using the Seurat package in R[49]. Single-droplet multiplets were detected using the union of two independent methods: Scrublet[50] and DoubletDetection[51]. Gene expression was normalized using NormalizeData, and the top 6,000 variable genes were identified using FindVariableFeatures, both with default parameters. The top variable genes were *z*-scored using ScaleData, and principal components (PCs) were computed using RunPCA for the top 200 PCs. The significance of each PC was computed using JackStraw, and heatmaps of the top cells and genes per PC were plotted using DimHeatmap; after reviewing both results the top 125 PCs were selected as features for clustering analysis. Clustering analysis was performed with the Louvain algorithm as implemented in Seurat[49] at resolutions 0.25, 0.5, 1 and 2. After reviewing the expression of known marker genes, we based our downstream analysis on the clustering results at resolution 1.

Cell-type determination

Primary cell types. To identify primary cell types, we used a transfer-learning approach based on scVI[52] and scANVI[28], in which reference dataset annotations are transferred to annotate subpopulations in a query dataset. Reference data were obtained from a previous study[30], which reported a human developmental forebrain dataset, and another study of the human hippocampus[11]. The latent representation was modelled using the top 5,000 most variable genes in the combined dataset and was corrected for batch effect based on the data source. We then used scANVI (v.1.0.3)[28] (n_samples_per_label=500) to transfer the most likely label from the reference datasets to the unannotated cells in our dataset. Based on the label transfer and gene marker annotations from clustering, we annotated astrocytes, neuroblasts, developmentally immature neurons, CA neurons, CA2–4 neurons, microglia, OPCs, mOLs, mGCs, endothelial cells and ependymal cells (Extended Data Fig. 6). NSCs were proposed to be part of the astrocyte cluster based on the recent literature[53]. Thus, astrocytes were provisionally labelled NSC/astrocyte.

Neuroblast and immature neurons. The primary cell-type analysis included cells identified as neuroblasts and developmentally immature neurons. To ensure the robustness of these annotations, we used previously published machine learning-based identification of immature neurons specifically in mGCs[11]. We then performed a subclustering analysis on cells identified as developmentally immature from the primary cell typing, which resulted in nine subclusters, and we performed a CytoTrace[54] analysis to infer the relative maturity stage of each cell type. We observed a clear distinction between neuroblasts and immature neurons, as well as clear correspondence between subclustered cells with either neuroblast or immature neurons (Extended Data Fig. 7a,b). Subclusters 0, 2 and 6 were reclassified as neuroblasts and combined with the other neuroblast cells, and subclusters 1, 3, 4, 5, 7 and 8 were reclassified as immature neurons and combined with other immature neurons.

NSCs. To differentiate astrocytes from NSCs, we performed a subclustering of the NSC/astrocyte population and an RNA velocity analysis using scVelo[55] on the NSC/astrocyte cluster along with neuroblasts, immature neurons and mGCs. Using the latent time measurement from the RNA velocity analysis, we identified a subcluster of the NSC/astrocyte population with the lowest latent time values (least differentiated) that was in between the remainder of the NSC/astrocyte cluster and the neurogenic cell types (Extended Data Fig. 1b,c). We identified these intermediate cells of NSC/astrocyte as the NSC subset, and the remainder as astrocytes.

Validation of the NSC signature

Systems analysis. Extended Data Fig. 1d,e and Supplementary Table 3 show the characterization of NSCs, neuroblasts and immature neurons based on the expression levels of developmental proxies (Extended Data Fig. 1d), the characterization of proxy expression trajectory in each cell type (Extended Data Fig. 1e) and open chromatin events of proxies in each cell type (Extended Data Fig. 1f). These were based on Supplementary Tables 5–7. We also computed differential gene and pathway analysis comparing NSCs to astrocytes. Pathway analysis revealed 57 pathways that were upregulated in NSCs, 23 of them are related to neuronal development, including axonal development, node of Ranvier, initial segment, growth cone, axonal guidance and dendritic spine (Supplementary Table 3).

We also compared NSC and astrocyte chromatin structure. We computed a UMAP of the ATAC–seq data of our NSC and astrocytes, which revealed that the NSCs have a chromatin structure that is distinct from astrocytes (Extended Data Figs. 1 and 4c).

Finally, SCENIC+ analysis was performed to study distinct GRNs (eRegulons) active in NSCs and mature astrocytes. This analysis also served as an orthogonal approach to assess whether the cells we annotated as NSCs represent a distinct population. This method integrates the chromatin accessibility and the expression of RNA at a single-cell level to infer the activity of TFs and to create GRNs. The regulon activity is an indicator of the activity of the TFs in GRNs. We found that NSCs and astrocytes formed distinct clusters based on the overall regulon embedding (Fig. 3a). This result further validates the annotation of NSCs as a distinct population. Diffusion analysis in the regulatory space of neurogenic cell types showed a clear developmental trajectory from NSCs to neuroblasts to immature neurons (Fig. 3b,c).

External comparisons. We compared NSCs in our dataset to one from a previous study[13], which also performed single-cell sequencing of the human hippocampus. In the previous study[13], the authors were able to identify both NSCs and neural progenitor cells. We identified the top 131 upregulated genes with adjusted $P < 0.05$ and $\log_2$[fold change] > 1 in the NSC/astrocyte population for our dataset and examined their expression levels in the other dataset[13]. Genes were selected only if they were expressed by >25% NSCs in both datasets. We observed that almost all of these genes were also upregulated in the NSCs of the previously published dataset relative to their astrocytes (Extended Data Fig. 2). This result illustrates a strong correspondence between the NSCs we identified and those independently obtained in the previous study[13].

To enable putative identification of NSCs more broadly, we derived a NSC signature scoring metric based on the 131 NSC upregulated genes, computed as the mean *z*-score over all astrocyte or NSC cells. We computed NSC scores using previously published data[13] and observed consistent high scores in their NSCs and low scores in their astrocytes (Extended Data Fig. 2). We also performed the reverse analysis, identifying upregulated genes in NSCs from the previously published data[13] using the same criteria as described above. This analysis identified 161 genes, 55 of which were common to the 131 genes from our data. We then computed the mean *z*-score of these 161 genes both in our NSC/astrocyte group and in the cells from the previous study[13] (Extended Data Fig. 2). We note that our NSCs also scored high using this approach,

which again indicated a strong concordance in how NSCs are differentiated from astrocytes.

We next applied our annotation approach to a dataset that should not contain any significant number of NSCs. We chose a previously published sequencing dataset of the human prefrontal brain[35]. We would not expect any significant presence of NSCs in the prefrontal cortex. After performing label transfer, using our data as a reference and annotating cells from the prefrontal brain dataset[35], a small number of apparent NSCs were labelled using this approach. However, when we examined the same 131 upregulated genes in NSCs in these cells, we observed a roughly even mix of upregulated and downregulated genes, which indicated that there is a lack of NSC signature and no defined population of NSCs (Extended Data Fig. 2).

Finally, we took a two-pronged approach and analysed two large datasets[33,34] using two different methods. For the first dataset[33], we examined each sample and tissue region, specifically those annotated as 'astrocytes', and used label transfer to predict NSCs. We reasoned that the similarity is highest between NSCs and astrocytes; therefore, populations that are typically labelled as astrocytes require in-depth analysis for possible subpopulations in the astrocyte cluster that might be NSCs. We did not observe any NSCs in any of the brain areas but did find a few modestly scoring cells in the pons for sample H19.30.002. Cells were labelled in red if their probability was >0.75 (Extended Data Fig. 7d). Label transfer is well-suited to broadly segregate and annotate cell populations based on a reference dataset. However, label transfer is not necessarily optimal for the identification of rare subpopulations, especially those that have high transcriptional similarity to larger subpopulations, as in the case for the large astrocyte population and the rarer NSC population. For the second dataset[34], we used our targeted approach, looking specifically at overexpression of NSC-specific genes relative to astrocytes and considering a holistic annotation across the neurogenic spectrum. We performed a NSC scoring analysis using the above 131-gene signature in the cell population identified as astrocytes using ROSMAP. This analysis was performed for all six brain regions, independently for each sample to avoid sample-to-sample differences from skewing gene expression *z*-scores (Extended Data Fig. 8). No NSCs were observed in any of the other brain areas other than a few in the anterior thalamus. Further annotation of immature neurons and mGCs by label transfer (using our data as a reference, annotating cells in ROSMAP) in the samples with positive NSCs showed that we were able to identify a significant number of both immature neurons and mGCs in the hippocampus, but we did not identify immature neurons or mGCs in the anterior thalamus (Extended Data Fig. 7c). From the combination of these observations, we conclude that our use of the NSC scoring procedure is specific for identifying NSCs, and that further holistic analysis of neurogenic cell types—in particular the identification of the immature and mGC end points—is crucial for a final determination of the neurogenic niche.

Validation of the neuroblast signature

We performed an additional global validation of NSC and neuroblast signatures in a comparison a previously published dataset[13]. We computed DEGs of NSCs and neuroblasts, this time relative to all other cells in the tissue, for both our data and the previously published data[13]. We compared the number of common DEGs ($\log_2$[fold change] > 1, adjusted $P < 0.05$, per cent expressed > 25%) of similarly annotated cells (NSCs in both or neuroblasts in both) and computed the statistical enrichment using Fisher's exact test. The overlap of DEGs for both NSCs and neuroblasts had large odds ratios and were highly significant. As a negative control, we considered the reverse comparison; that is, overlap of DEGs in NSCs in one dataset to those from neuroblasts in the other dataset; these were not significant and had odds ratios close to 1 (Supplementary Table 4). Together, these analyses show commonality in the gene sets in our NSC and neuroblast cell types compared with the previously published dataset[13] and confirm that NSCs and neuroblasts are also distinct from each other.

We also performed additional specific comparisons to highlight differences between neuroblasts and oligodendrocytes, which have broadly similar transcriptional profiles. We show the expression levels of selected proxies of neuroblasts and oligodendrocytes in a dot plot (Extended Data Fig. 2a). We also computed DEGs and pathway enrichment of for neuroblasts versus mOLs. Pathway analysis revealed 169 pathways that were upregulated in neuroblasts. Of these, 80 pathways were directly related to axonal, dendritic and presynaptic and postsynaptic structure, function and plasticity (Supplementary Table 2). Finally, we performed an RNA velocity analysis over the population of neuroblasts and mOLs and observed a consistently lower latent time estimation for the neuroblast population, again reinforcing the relative level of differentiation of these cells (Extended Data Fig. 7a, b).

Peak recalling

After determination of cell types, we re-called peaks separately for each cell type using Seurat[49], merging peaks across all cell types to obtain a more complete measurement of the open chromatin peaks for rarer cell types.

Cell-type abundance and statistical analysis

We counted the total cells per cell type per sample and computed association statistics between these cell counts and diagnosis of the participants and other AD-related traits using edgeR[56] without the TMM normalization. Comparisons between groups, for example, cell abundance between AD and HA, were computed using the exactTest function[56]. Association of cell-type abundance with continuous variables, such as cognitive scores, were computed using generalized linear models. *P* values were adjusted for multiple testing using FDR correction.

Differential gene expression between clusters

DEGs for each neurogenic cell type were obtained using the FindAllMarkers function in Seurat[49] with the Wilcox test, comparing each cell type to all other cells. This analysis was performed between NSCs, neuroblasts and immature neurons only. Significantly DEGs were determined based on adjusted $q < 0.05$.

Differential gene and peak expression by diagnosis

Differential gene and peak statistics between diagnosis groups were computed using a pseudo-bulk approach. Counts for gene expression or open chromatin were summed for each sample across all cells in a given cluster. Low-expressed genes or peaks—expressed in fewer than 25% of samples or with fewer than 50 total counts across all samples—were removed. Differential expression and open chromatin statistics for each cluster were computed using edgeR using the exactTest[56] to perform pairwise between groups. *P* values were adjusted using FDR correction. DEGs were determined based on FDR < 0.05.

Motif analysis of differentially expressed peaks

Motif enrichment analysis enables inference of specific TFs that are driving developmental changes between clusters. First, we searched for instances of known TF motifs in all peak sequences from the JASPAR database[57] using FIMO[58]. Then we computed motif enrichment statistics for each set of differentially expressed peaks by comparing the fraction of motif-containing peaks in or not in the differentially expressed peaks using Fisher's exact test. We repeated this test for all motifs, correcting for multiple testing using the BH-corrected FDR[59].

Pathway analysis of DEGs

Pathway enrichment of DEGs was interrogated against the Neuroimmune Gene Ontology (NIGO) Biological Process (BP) pathway database. Pathway enrichment for DEGs was performed with Fisher's exact test in R. *P* values were adjusted for multiple testing using FDR correction.

GRN analysis

Regulatory interactions between TFs and target genes through open chromatin were determined using a similar TF–peak–gene trio approach to that as previously described[39]. First, low-expressed genes (expressed in <10% of cells) and peaks (observed in <2% of cells) were removed. Potential peak–gene interactions were identified by annotating each peak to all genes within 200 kb or overlapping the body of the gene. TF–peak interactions were identified by searching for TF motifs from the JASPAR core vertebrate database[60] in open chromatin regions using FIMO[61] with motif $P < 1 \times 10^{-5}$. Peak and gene log-normalized expression levels were averaged over the 20 nearest neighbours.

Potential regulatory interactions from TF gene–peak–target gene trios were constructed on the basis of TF–peak binding and peak–gene proximity in the genome, and Pearson's correlation coefficients were computed on the normalized expression for each pair. TF gene–peak correlation coefficients less than zero were set to 0, and the inferred type of TF–target gene regulatory interaction (activation or repression) was based on the sign of the TF gene–target gene correlation. To rank and prioritize the interactions based on those with the strongest evidence, we computed the geometric mean of the absolute value of the three correlation coefficients. To scale this score with respect to the direction of regulation, we multiplied the score by the sign of the TF gene–target gene correlation.

For GRN analysis of neurogenic cell types (NSCs, neuroblasts and immature neurons), we performed this analysis separately for cells from each diagnosis group (YA, HA, PCI, AD and SA) to enable comparisons of interaction scores between cell types. We also augmented the above-computed scores with the differential gene and peak statistics computed between cell types. For each cell type, we looked at the log fold change values in TF gene, peak and target gene expression. First, we verified that the sign of each correlation coefficient matched the sign of the product of the $\log_2$[fold change] values. Second, we computed the geometric mean of the absolute value of all three $\log_2$[fold change] values to obtain a cell-type-specific score.

eRegulon analysis to investigate GRNs

We ran SCENIC+ with region sets built from the 3,000 NTOP topics, OTSU topics, DARs between cell types and DARs between conditions in individual cell types. We used a custom *cis*-target database created with 1,000-base-pair padding from every region present in our filtered ATAC modality. Input motifs were taken from v10nr_clust-nr.hgnc. We generated these inputs separately for all cell types and neurogenic cell types. Both sets of inputs were independently processed through SCENIC+ using default parameters[40].

Cell–cell interaction

Interactions between cell types were inferred using the CellChat[62] package in R with default parameters for cells from astrocytes, CA neurons and neurogenic cells (NSCs, neuroblasts and immature neurons grouped together). An initial analysis was conducted over all cells from all diagnosis groups. A second analysis was conducted separately for each biological sample. In the second per-sample analysis, we quantified the same interactions that were identified in the first overall analysis to enable a fair comparison of interaction strengths from sample-to-sample. Differential statistics of the interaction probabilities was computed using limma in R[63].

Resilience analysis

Specific filtering for 'SA resilience' genes and peaks was based on differential gene and peak expression by diagnosis results. AD–YA, AD–HA and SA–AD pairs were compared and then a summarized effect and significance statistic was computed as $\log_2$[fold change] × $-\log_{10}[q]$. All three comparisons were required to have the same sign (same direction). A summary score was computed as the geometric mean of the absolute value of all three summary statistics.

Healthy ageing analysis

Specific filtering for healthy versus unhealthy ageing, by comparing PCI and SA outcomes, was also based on differential gene and peak expression by diagnosis results. In this case, we looked for genes and peaks for which the SA–HA result is opposite to PCI–HA and PCI–YA, and that at least one of these comparisons had $q < 0.2$.

For CellChat healthy ageing interactions, we obtained interactions that were significantly altered in AD but displayed the same relative directionality in SA–HA, PCI–HA, and PCI–YA.

Reporting summary

Further information on research design is available in the Nature Portfolio Reporting Summary linked to this article.

Data availability

Raw and processed datasets associated with this study are publicly available from the Gene Expression Omnibus at accession number GSE268609 (https://www.ncbi.nlm.nih.gov/geo/query/acc.cgi?acc=GSE268609). Source data are provided with this paper.

44. Montine, T. J. et al. National Institute on Aging-Alzheimer's Association guidelines for the neuropathologic assessment of Alzheimer's disease: a practical approach. *Acta Neuropathol.* **123**, 1–11 (2012).
45. Hyman, B. T. et al. National Institute on Aging-Alzheimer's Association guidelines for the neuropathologic assessment of Alzheimer's disease. *Alzheimers Dement.* **8**, 1–13 (2012).
46. Rey, S. M. *Auditory Verbal Learning Test: A Handbook* (Western Psychological Services, 2004).
47. Shirk, S. D. et al. A web-based normative calculator for the uniform data set (UDS) neuropsychological test battery. *Alzheimers Res. Ther.* **3**, 32 (2011).
48. Heaton, R., Miller, S., Taylor, M. & Grant, I. *Revised Comprehensive Norms for an Expanded Halstead-Reitan Battery: Demographically Adjusted Neuropsychological Norms for African American and Caucasian Adults* (Psychological Assessment Resources, 2004).
49. Butler, A., Hoffman, P., Smibert, P., Papalexi, E. & Satija, R. Integrating single-cell transcriptomic data across different conditions, technologies, and species. *Nat. Biotechnol.* **36**, 411–420 (2018).
50. Wolock, S. L., Lopez, R. & Klein, A. M. Scrublet: computational identification of cell doublets in single-cell transcriptomic data. *Cell Syst.* **8**, 281–291 (2019).
51. Shor, J. JonathanShor/DoubletDetection: doubletdetection v4.3.0.post1. *Zenodo* https://doi.org/10.5281/zenodo.14827937 (2025).
52. Gayoso, A. et al. A Python library for probabilistic analysis of single-cell omics data. *Nat. Biotechnol.* **40**, 163–166 (2022).
53. Kempermann, G., Jessberger, S., Steiner, B. & Kronenberg, G. Milestones of neuronal development in the adult hippocampus. *Trends Neurosci.* **27**, 447–452 (2004).
54. Gulati, G. S. et al. Single-cell transcriptional diversity is a hallmark of developmental potential. *Science* **367**, 405–411 (2020).
55. Bergen, V., Lange, M., Peidli, S., Wolf, F. A. & Theis, F. J. Generalizing RNA velocity to transient cell states through dynamical modeling. *Nat. Biotechnol.* **38**, 1408–1414 (2020).
56. Robinson, M. D., McCarthy, D. J. & Smyth, G. K. edgeR: a Bioconductor package for differential expression analysis of digital gene expression data. *Bioinformatics* **26**, 139–140 (2010).
57. Khan, A. & Mathelier, A. JASPAR RESTful API: accessing JASPAR data from any programming language. *Bioinformatics* **34**, 1612–1614 (2018).
58. Bailey, T. L. et al. MEME SUITE: tools for motif discovery and searching. *Nucleic Acids Res.* **37**, W202–W208 (2009).
59. Benjamini, Y. & Hochberg, Y. Controlling the False discovery rate: a practical and powerful approach to multiple testing. *J. R. Stat. Soc.* **57**, 289–300 (2018).
60. Rauluseviciute, I. et al. JASPAR 2024: 20th anniversary of the open-access database of transcription factor binding profiles. *Nucleic Acids Res.* **52**, D174–D182 (2024).
61. Grant, C. E., Bailey, T. L. & Noble, W. S. FIMO: scanning for occurrences of a given motif. *Bioinformatics* **27**, 1017–1018 (2011).
62. Jin, S. et al. Inference and analysis of cell–cell communication using CellChat. *Nat. Commun.* **12**, 1088 (2021).
63. Ritchie, M. E. et al. limma powers differential expression analyses for RNA-sequencing and microarray studies. *Nucleic Acids Res.* **43**, e47 (2015).

Acknowledgements Bioinformatic analyses were performed by staff at the UIC Research Informatics Core, a department supported in part by NCATS through grant UM1TR005438. This work was supported by NIA AG033570, AG033570-S2, AG076940, AGO79002, AG060238 and AG061628 (to O.L.), R01-AG091545(JR) and T32 HL139439 (to M.A.S.), F31AG090005 (to M.A.S.), a UI College of Medicine Team Science Award (to O.L. and J.R.), and the Nancy and Buster Alvord endowment (to C.D.K.). Brain donors and tissue resources were supported by the UW Alzheimer's Disease Research Center (P30 AG066509), the Adult Changes in Thought (ACT) study (U19 AG066567) and the Pacific Northwest Brain Donor Network (supported by

funds from NIH UM1 MH130981, UM1 MH134812, U01 NS137500 and U01 NS137484, U24 AG072458, DoD W81XWH-21-S-TBIPH2, the Allen Institute for Brain Science and the Northwestern University Alzheimer's Disease Research Center (P30AG072977), the SuperAging Research Initiative (U19AG073153), the Karen Toffler Charitable Trust and the Gefen-Querrey Brain Health Fund). The authors thank H. Song for help with the implementation of the machine learning approach and A. Schantz, J. Campos, E. Ragaglia, A. Wilson and M. Damodarasamy for outstanding data and technical support. This work would be impossible without the incredible generosity of brain donors and their loved ones.

Author contributions O.L. designed the research, analysed data and wrote the manuscript. A.D. conducted all experiments, acquired and analysed data and wrote the manuscript. K.R.S. and M.M.M. sorted and collected tissue samples for sequencing. I.A.A., C.D.K.,C.G., M.-M.M. and D.A.B. provided the samples. S.W. and T.G. conducted clinical tests for determination of cognitively age-normal versus cognitively age-above normal individuals. Y.Z., Y.L., M.A.S., M.M.-C. and J.R. analysed data. All authors critically revised and approved the manuscript.

Competing interests The authors declare no competing interests.

Additional information

Supplementary information The online version contains supplementary material available at https://doi.org/10.1038/s41586-026-10169-4.

Correspondence and requests for materials should be addressed to Jalees Rehman or Orly Lazarov.

Peer review information *Nature* thanks the anonymous reviewers for their contribution to the peer review of this work.

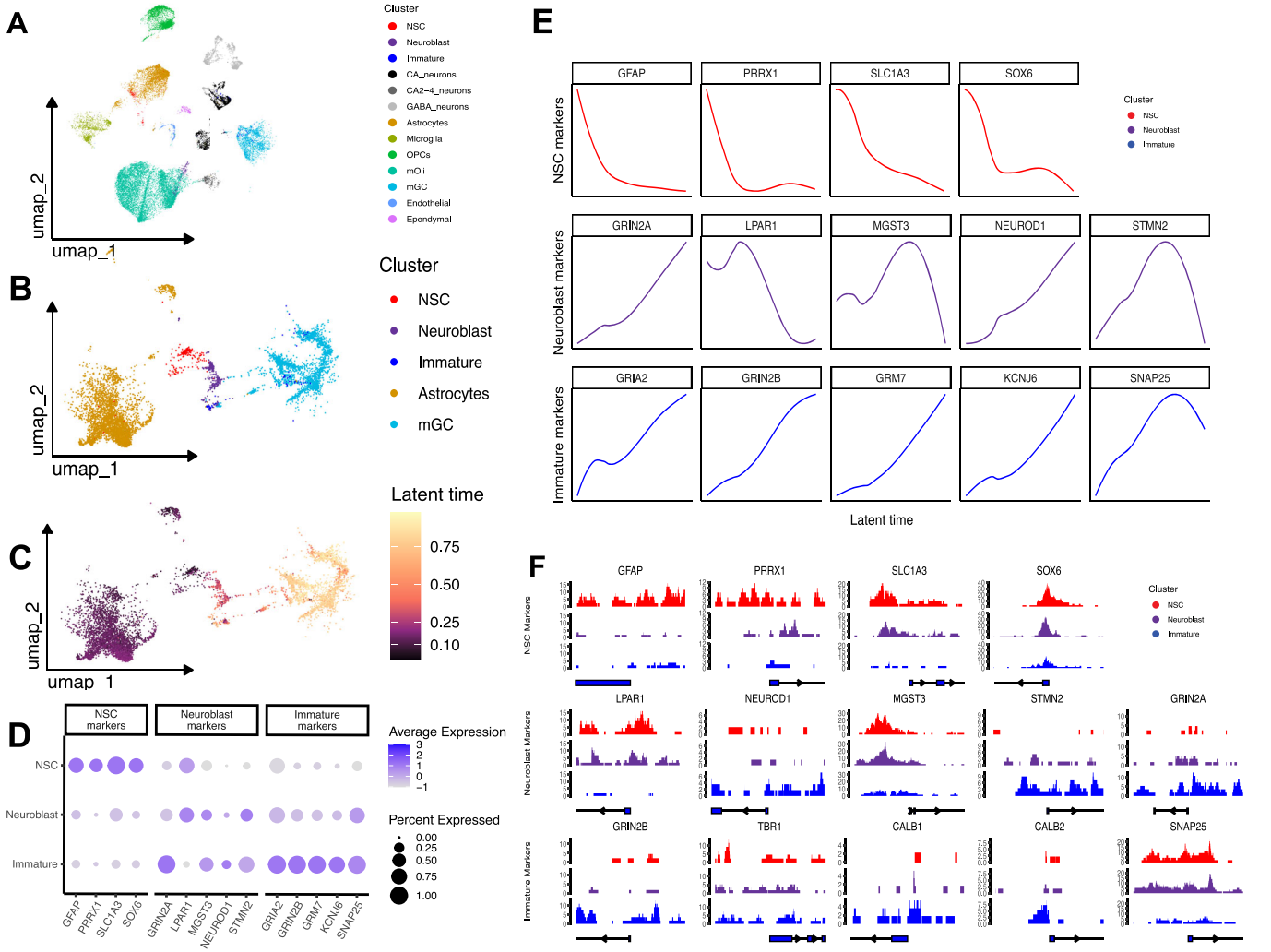

Extended Data Fig. 1 | Neurogenesis trajectory in the human adult hippocampus. A. UMAP of all cell types for all YA cells. **B**. UMAP of astrocytes, neurogenic cell types and mature granule neurons (mGC), which have broad transcriptional similarity to NSCs, neuroblasts and immature neurons. **C**. Latent time of RNA velocity, showing earliest time points for NSCs, and development from there towards astrocytes in one direction, and neuroblast/immature/mGC in the other direction. **D**. Dotplot showing expression of neurogenesis-related marker genes in neurogenic cell types (NSC, neuroblast, immature). **E**. Smoothed gene expression over latent time for neurogenesis-related marker genes, across all neurogenic cell types. **F**. Open chromatin (counts per billion bases) around gene promoters (+/2 kb from TSS) for neurogenesis-related marker genes over neurogenic cell types.

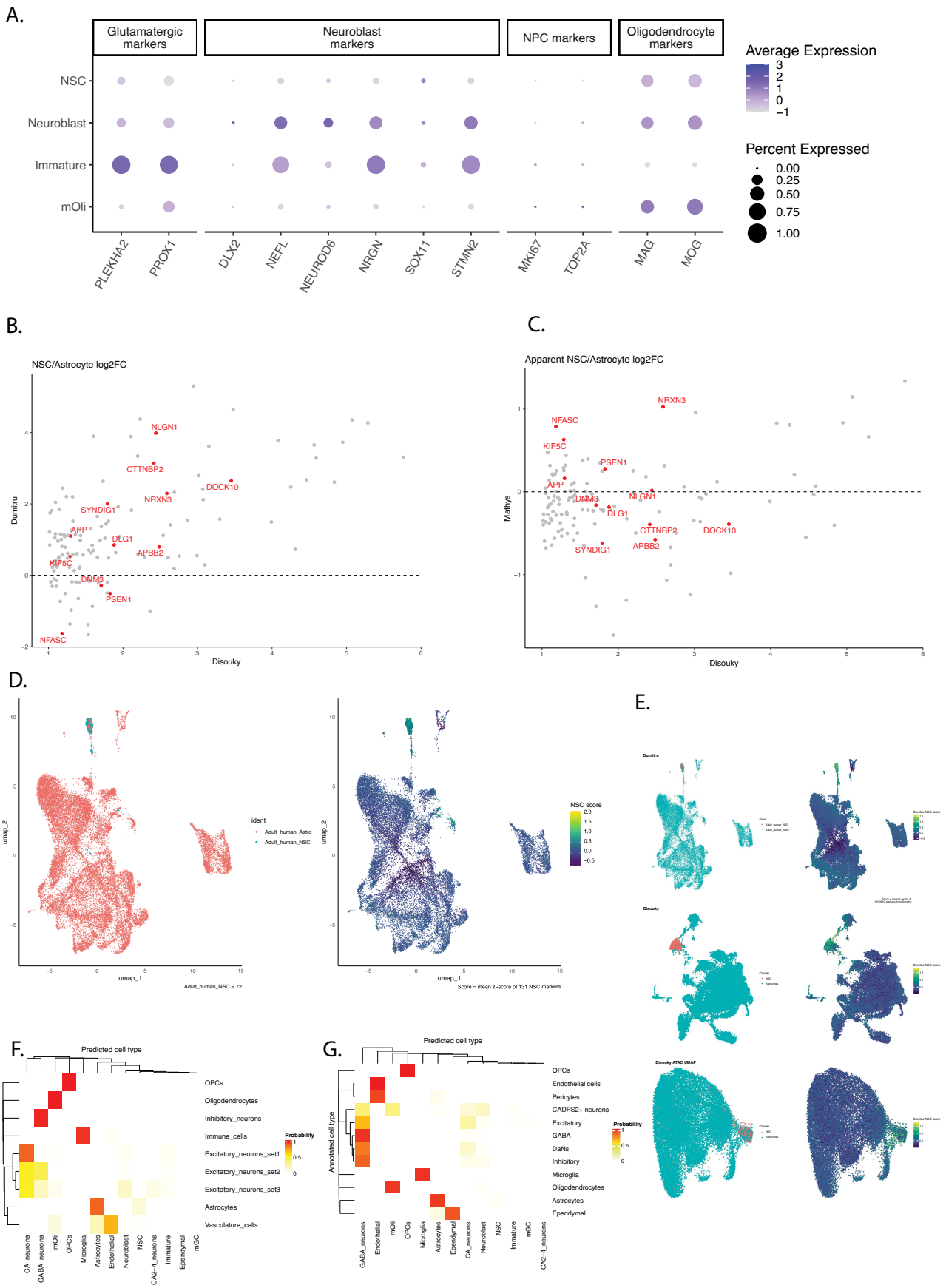

Extended Data Fig. 2 | See next page for caption.

Extended Data Fig. 2 | Cell type validation. A. Dotplot of expression levels of neuroblasts and oligodendrocyte proxies observed in a single-cell transcriptomics-based human brain atlas. **B,C**. NSC_versus_astrocyte_DEGs signature. Average predicted probability of label transfer per cell type in the Dumitru et al. dataset[13] (B) or Mathys et al. dataset[35] (C) based on the current study's signature, i.e., top 131 upregulated genes with p_adj<0.05 and log2FC > 1 in NSC/Astrocyte. In (B) we observed that the vast majority of top NSC genes in the current study were also upregulated in the NSCs identified in Dumitru et al. dataset[13]. In contrast, in (C) a strong correspondence between the same cell types, and absence of predicted mGC, immature, CA2-4, neuroblast and NSC was observed. **D**. Left: UMAP of Dumitru et al. dataset[13] astrocytes and NSCs. Right: Mean z-score per cell for all astrocytes and NSCs from the Dumitru et al. data based on top NSC genes in the current study. We observed high scoring compatibility between the studies. **E**. Reverse scoring approach. Top panel "Dumitru": Top DEGs NSC versus astrocytes in the Dumitru et al. data[13] using the same threshold parameters as in the current study. Middle panel "Disouky": astrocytes and NSC in the current study scored based on top DEGs identified in the Dumitru et al. data[13]. Low panel "Disouky ATAC UMAP": NSC and Astrocyte in the current study in a UMAP computed from the ATACseq data showing a distinct chromatin of NSCs from astrocytes. **F,G**. Lack of neurogenic cell types in other brain regions. Comparison of the current study to Mathys et al. dataset[35] (F) and Smajic et al. dataset[36] (G). Average predicted probability of label transfer per cell type showed weak correspondence of hippocampal neurogenesis in these studies.

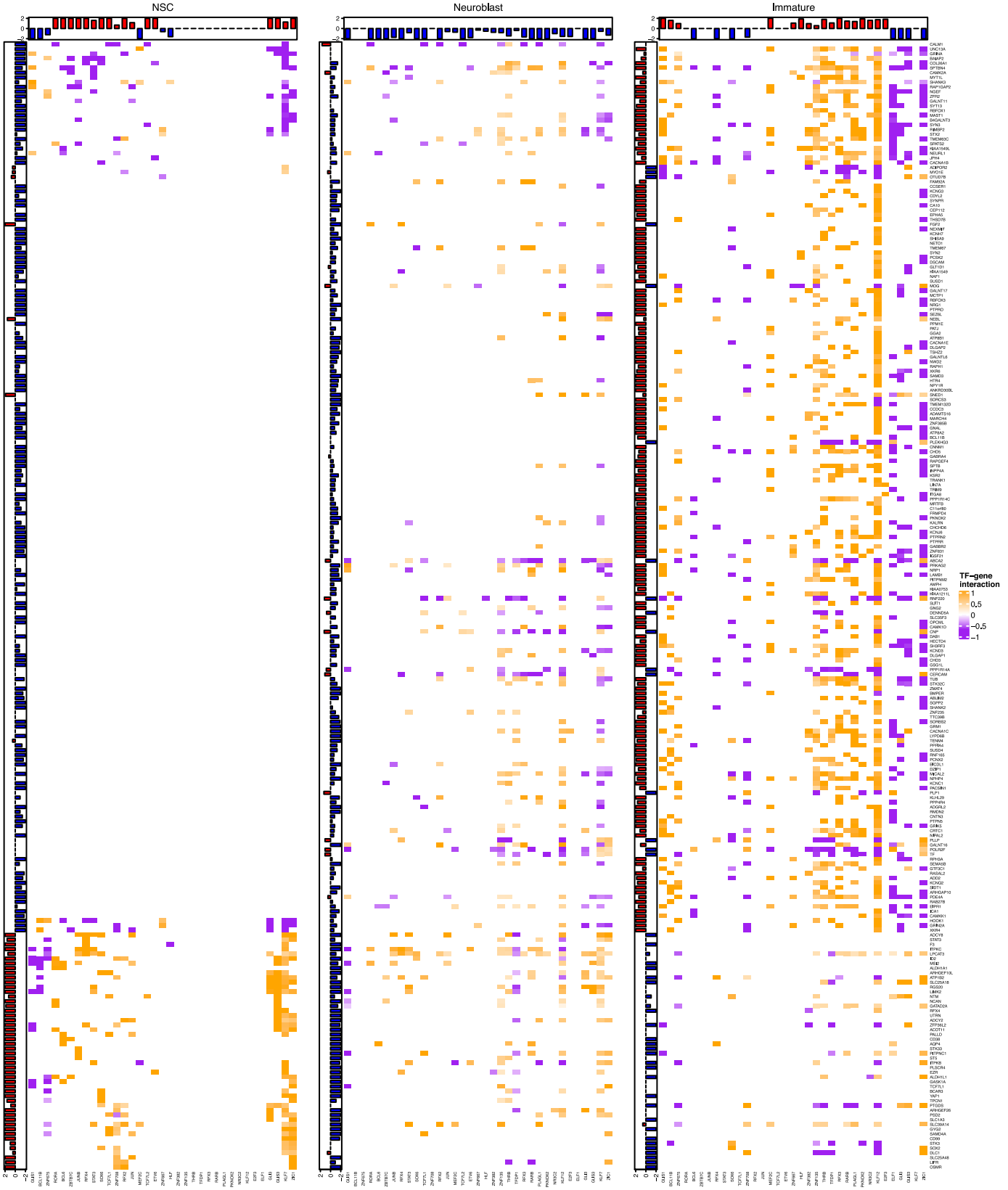

Extended Data Fig. 3 | Gene regulatory networks (GRNs) of neurogenesis in the Young Adult cohort. This analysis was performed using the TF–peak–gene trios approach[38].Interactions in NSCs were downregulated in neuroblasts and further downregulated in immature neurons. In contrast, interactions that did not exist in NSCs, were upregulated in neuroblasts and to a greater extent in immature neurons.

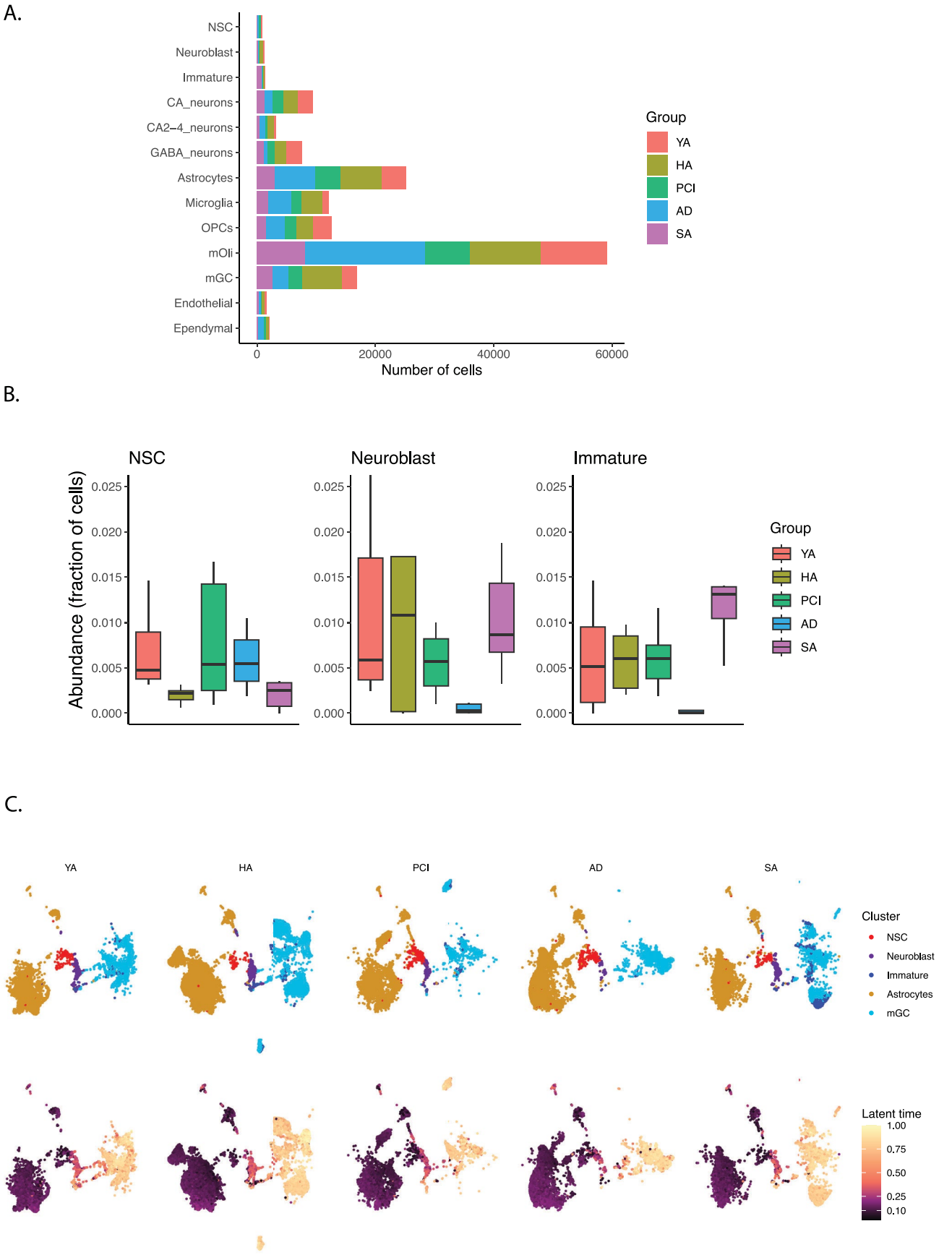

Extended Data Fig. 4 | A. Number of cells as a function of diagnosis. **B.** Cell abundance as a function of diagnosis. **C.** Latent time of RNA velocity of NSC, neuroblasts, immature neurons, mGCs and astrocytes as a function of diagnosis.

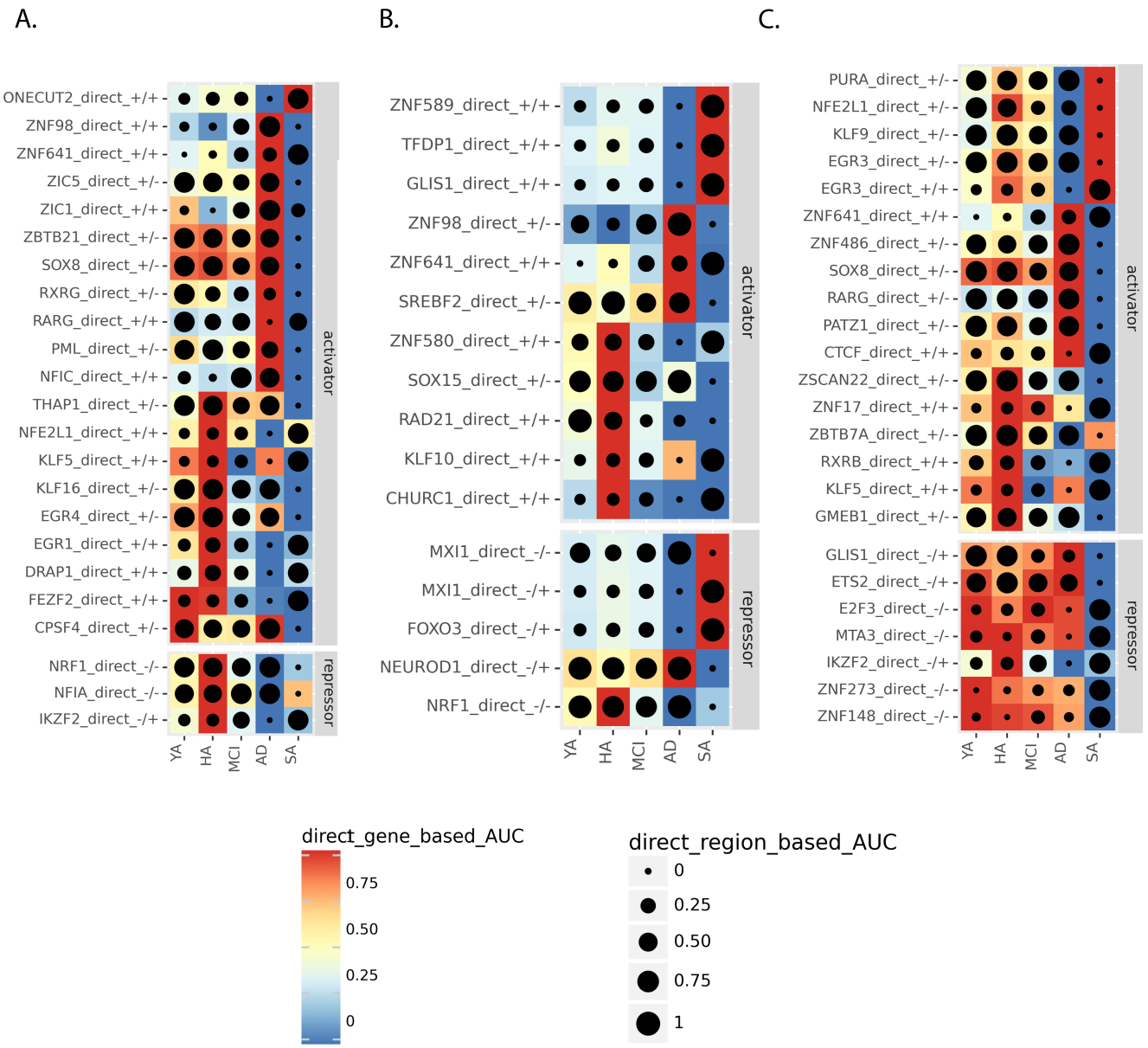

Extended Data Fig. 5 | A-C. eRegulons of neurogenesis in all conditions. A. NSCs. **B.** Neuroblasts. **C.** Immature neurons.

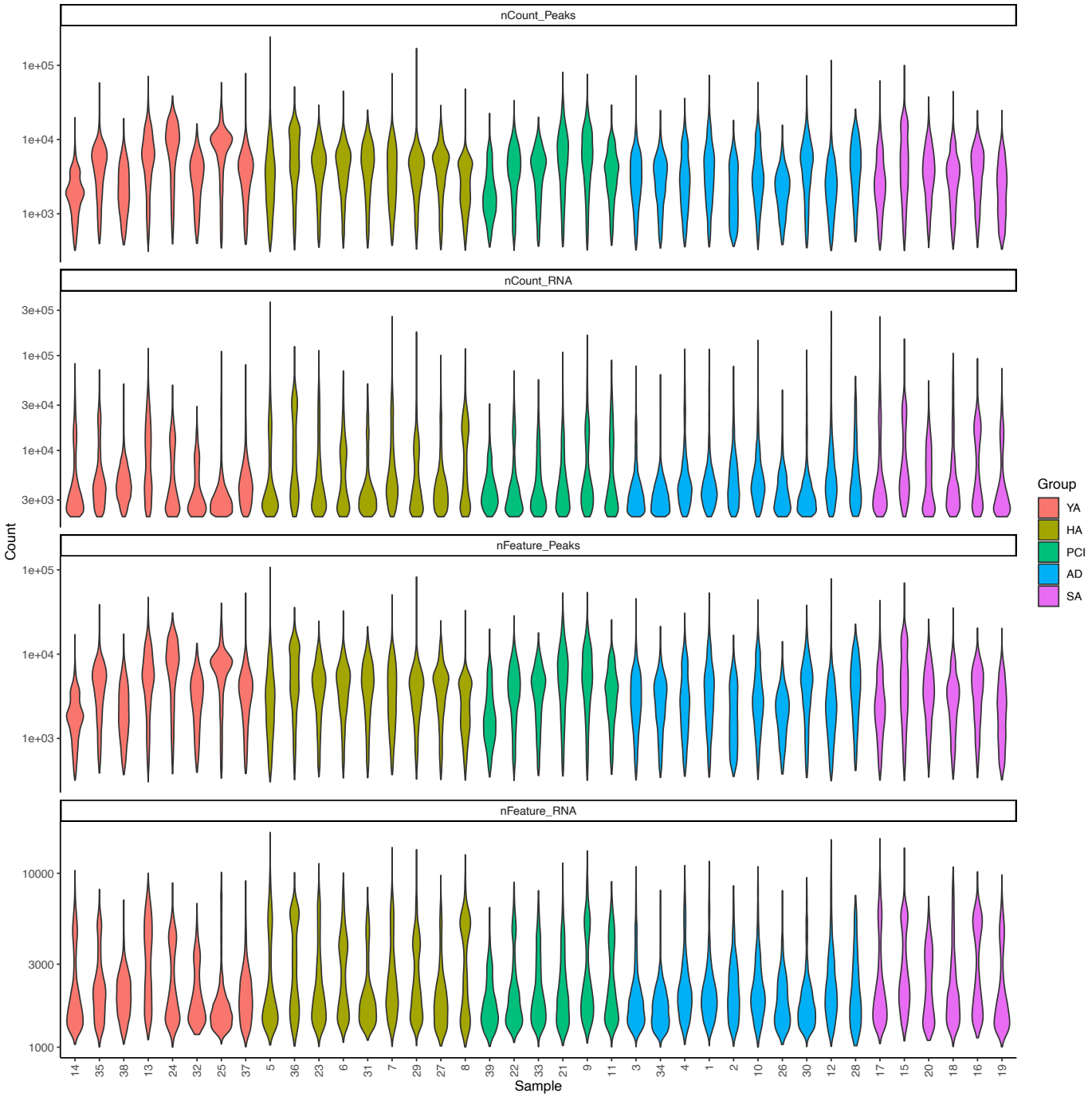

Extended Data Fig. 6 | QC metrics per sample. Violin plots of QC metrics per sample, colored by group; nCount_Peaks = total counts over all peaks per cell; nCount_RNA = total counts over all genes per cell; nFeature_Peaks = total peaks observed per cell with at least one count; nFeature_RNA = total genes expressed per cell with at least one count. No systematic shifts in sample or cell quality per group that would result in bias or misleading results in the downstream analysis were observed.

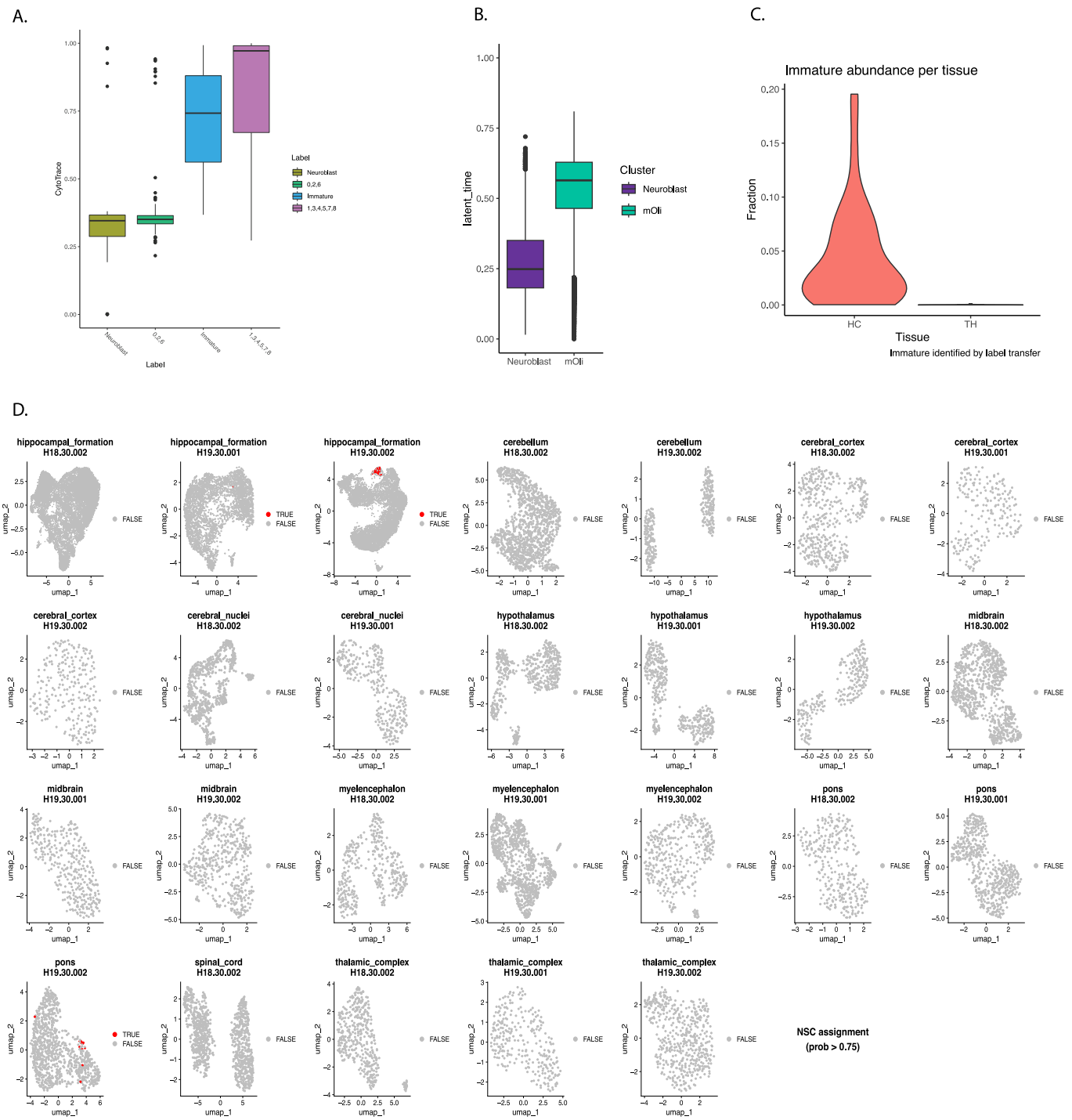

Extended Data Fig. 7 | Additional neurogenic signature validation. **A**. Neuroblasts versus immature neurons. Illustrates the final determination of neuroblasts and immature neurons in the current study. "Developmental immature" cell labels from the initial label transfer were clustered based on a comparison with their developmental "time" (CytoTRACE) as neuroblasts or immature neurons, the latter were determined based on machine learning[11]. **B**. Velocity of neuroblast versus oligodendrocytes. Latent time from RNA velocity analysis of neuroblast and oligodendrocytes. **C**. Abundance of immature neurons in the hippocampus in the current study and in the thalamus of Liu et al. dataset[34]. The annotation of immature neurons and mature granule cells (mGC) in the ROSMAP data was done by label transfer using our dataset as a reference. Annotation was done in the anterior thalamus samples with positive NSCs (see Extended Data Fig. 8). The data showed the identification of a significant number of both immature neurons and mGC in the hippocampus, but none in the anterior thalamus. **D**. Examination of the current neurogenic signature in Siletti et al. dataset[33]. Each sample and tissue region from the Siletti datasets, specifically those annotated as "astrocytes", was examined using label transfer to predict NSCs. We observed no NSC in any of the brain areas but did find a few modestly scoring cells in the pons for H19.30.002. Cells were labeled in red if their probability was >0.75. However, our identification of NSCs did not rely on the label transfer approach.

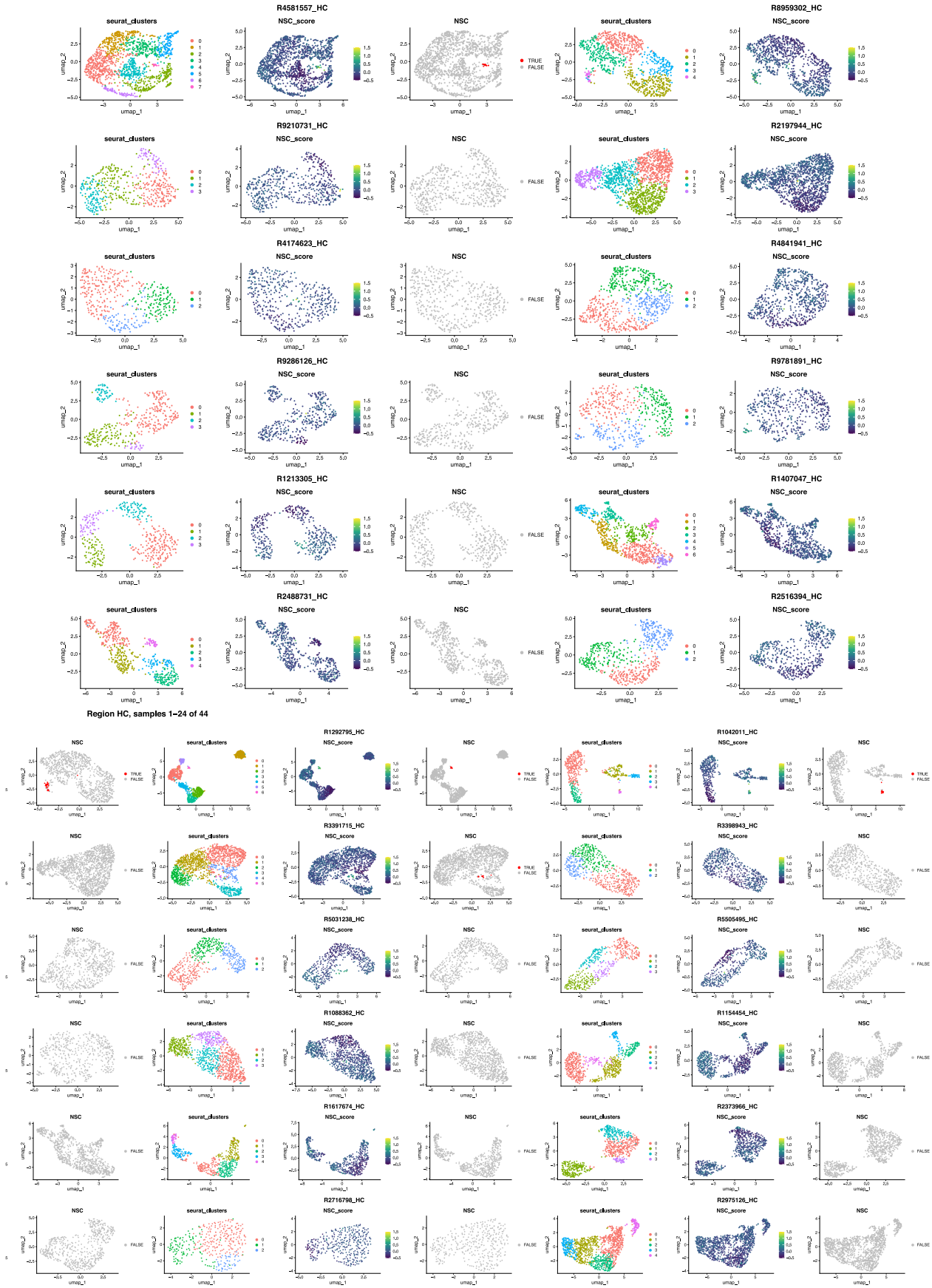

Extended Data Fig. 8 | See next page for caption.

Extended Data Fig. 8 | Additional neurogenic signature validation. Examination of the current neurogenic signature in Liu et al. dataset[34]. This data set has 377 total samples from 111 donors in 6 different brain regions. An NSC scoring analysis using the current study's 131-gene signature in the cell population identified as "astrocytes" by ROSMAP dataset; this analysis was performed for all six brain regions, independently for each sample to avoid sample-to-sample differences from skewing gene expression z-scores. The figure shows a UMAP plot for astrocytes for each sample in each tissue. Three panels per sample per tissue in this plot, from left-to-right: Clustering was performed at resolution 0.5 in Seurat. The NSC score was examined for each cell, and clusters with an average z score > 0.5 were identified as NSCs. We observed NSCs in several hippocampal datasets using this procedure. No NSCs were observed in any of the other brain areas other than a few in the anterior thalamus. For the latter region, no immature neurons were observed.

nature portfolio

Corresponding author(s): Orly Lazarov

Last updated by author(s): 01/16/2026

Reporting Summary

Nature Portfolio wishes to improve the reproducibility of the work that we publish. This form provides structure for consistency and transparency in reporting. For further information on Nature Portfolio policies, see our Editorial Policies and the Editorial Policy Checklist.

Statistics

For all statistical analyses, confirm that the following items are present in the figure legend, table legend, main text, or Methods section.

n/a	Confirmed	
☐	☒	The exact sample size (*n*) for each experimental group/condition, given as a discrete number and unit of measurement
☐	☒	A statement on whether measurements were taken from distinct samples or whether the same sample was measured repeatedly
☐	☒	The statistical test(s) used AND whether they are one- or two-sided *Only common tests should be described solely by name; describe more complex techniques in the Methods section.*
☐	☒	A description of all covariates tested
☐	☒	A description of any assumptions or corrections, such as tests of normality and adjustment for multiple comparisons
☐	☒	A full description of the statistical parameters including central tendency (e.g. means) or other basic estimates (e.g. regression coefficient) AND variation (e.g. standard deviation) or associated estimates of uncertainty (e.g. confidence intervals)
☐	☒	For null hypothesis testing, the test statistic (e.g. *F*, *t*, *r*) with confidence intervals, effect sizes, degrees of freedom and *P* value noted *Give P values as exact values whenever suitable.*
☒	☐	For Bayesian analysis, information on the choice of priors and Markov chain Monte Carlo settings
☒	☐	For hierarchical and complex designs, identification of the appropriate level for tests and full reporting of outcomes
☐	☒	Estimates of effect sizes (e.g. Cohen's *d*, Pearson's *r*), indicating how they were calculated

Our web collection on statistics for biologists contains articles on many of the points above.

Software and code

Policy information about availability of computer code

Data collection	bcl2fastq embedded by Illumina
Data analysis	cellranger-arc (https://www.10xgenomics.com/support/software/cell-ranger-arc/latest), v2.0.0 Seurat (https://satijalab.org/seurat/), v4.0.5 scVI (10.1038/s41587-021-01206-w), v1.0.3 scANVI (doi.org/10.15252/msb.20209620), v1.0.3 edgeR (https://bioconductor.org/packages/release/bioc/html/edgeR.html), v3.36.0 fimo (https://meme-suite.org/meme/doc/fimo.html), v5.4.1 monocle (http://cole-trapnell-lab.github.io/monocle-release/docs/), v2.22.0 fastTopics (https://stephenslab.github.io/fastTopics/), v0.6-142 GSEA (https://www.gsea-msigdb.org/gsea/index.jsp), v4.1.0 CellChat (https://github.com/jinworks/CellChat), v1.6.1 NeuronChat (https://github.com/Wei-BioMath/NeuronChat), v.1.0.0

For manuscripts utilizing custom algorithms or software that are central to the research but not yet described in published literature, software must be made available to editors and reviewers. We strongly encourage code deposition in a community repository (e.g. GitHub). See the Nature Portfolio guidelines for submitting code & software for further information.

Data

Policy information about availability of data

All manuscripts must include a data availability statement. This statement should provide the following information, where applicable:

- Accession codes, unique identifiers, or web links for publicly available datasets
- A description of any restrictions on data availability
- For clinical datasets or third party data, please ensure that the statement adheres to our policy

https://www.ncbi.nlm.nih.gov/geo/query/acc.cgi?acc=GSE268609

Research involving human participants, their data, or biological material

Policy information about studies with human participants or human data. See also policy information about sex, gender (identity/presentation), and sexual orientation and race, ethnicity and racism.

Reporting on sex and gender	This study uses de-identified postmortem frozen hippocampi. We reported sex, age and all criteria related to brain pathology.
Reporting on race, ethnicity, or other socially relevant groupings	This study did not report these social parameters. N/A
Population characteristics	N/A. This study did not recruit patients/population.
Recruitment	N/A. This study did not recruit patients/population.
Ethics oversight	UIC IRB, University of Washington IRB

Note that full information on the approval of the study protocol must also be provided in the manuscript.

Field-specific reporting

Please select the one below that is the best fit for your research. If you are not sure, read the appropriate sections before making your selection.

☒ Life sciences ☐ Behavioural & social sciences ☐ Ecological, evolutionary & environmental sciences

For a reference copy of the document with all sections, see nature.com/documents/nr-reporting-summary-flat.pdf

Life sciences study design

All studies must disclose on these points even when the disclosure is negative.

Sample size	n=10 hippocampi of Alzheimer's disease, n= 8 each for young adults with intact memory (YA) and aged adults with no cognitive impairments (HA), n= 6 each for patients of preclinical with intermediate pathology (PCI) and individuals with extraordinary memory capacity (SuperAgers or SA) . A total of 355,997 nuclei were sequenced. The maximun sample size available from brain banks was used.
Data exclusions	For sequencing, cells with >10% mitochondrial expression; cells with low numbers of genes expressed (<1000 genes) or low total UMI RNA counts (<2000 UMI counts); and cells with low peak numbers (<200 peaks) or total ATAC counts (<500 counts) were removed
Replication	*Sequencing QC, validation of observations against previous datasets.*
Randomization	De-identified samples were obtained from the Alzheimer's disease research centers at University of Washington and the Northwestern University Alzheimer's Disease Research Center (NU-ADRC) Brain Bank. Samples were selected by the Alzheimer's centers based on cognitive diagnosis and Alzheimer's pathology.
Blinding	Samples that arrived from the Alzheimer's disease centers were coded. Investigators , sequencing researchers and analysts were blinded to codes.

Reporting for specific materials, systems and methods

We require information from authors about some types of materials, experimental systems and methods used in many studies. Here, indicate whether each material, system or method listed is relevant to your study. If you are not sure if a list item applies to your research, read the appropriate section before selecting a response.

Materials & experimental systems

n/a	Involved in the study
☒	☐ Antibodies
☒	☐ Eukaryotic cell lines
☒	☐ Palaeontology and archaeology
☒	☐ Animals and other organisms
X	☐ Clinical data
☒	☐ Dual use research of concern
☒	☐ Plants

Methods

n/a	Involved in the study
☒	☐ ChIP-seq
☒	☐ Flow cytometry
☒	☐ MRI-based neuroimaging

Clinical data

Policy information about clinical studies

All manuscripts should comply with the ICMJE guidelines for publication of clinical research and a completed CONSORT checklist must be included with all submissions.

Clinical trial registration	*Provide the trial registration number from ClinicalTrials.gov or an equivalent agency.*
Study protocol	*Note where the full trial protocol can be accessed OR if not available, explain why.*
Data collection	*Describe the settings and locales of data collection, noting the time periods of recruitment and data collection.*
Outcomes	*Describe how you pre-defined primary and secondary outcome measures and how you assessed these measures.*

Plants

Seed stocks	*Report on the source of all seed stocks or other plant material used. If applicable, state the seed stock centre and catalogue number. If plant specimens were collected from the field, describe the collection location, date and sampling procedures.*
Novel plant genotypes	*Describe the methods by which all novel plant genotypes were produced. This includes those generated by transgenic approaches, gene editing, chemical/radiation-based mutagenesis and hybridization. For transgenic lines, describe the transformation method, the number of independent lines analyzed and the generation upon which experiments were performed. For gene-edited lines, describe the editor used, the endogenous sequence targeted for editing, the targeting guide RNA sequence (if applicable) and how the editor was applied.*
Authentication	*Describe any authentication procedures for each seed stock used or novel genotype generated. Describe any experiments used to assess the effect of a mutation and, where applicable, how potential secondary effects (e.g. second site T-DNA insertions, mosiacism, off-target gene editing) were examined.*